Chemical Science

ROYAL SOCIETY OF CHEMISTRY

REVIEW

View Article Online
View Journal | View Issue

Cite this: *Chem. Sci.*, 2024, **15**, 18751

The chirality-induced spin selectivity effect in asymmetric spin transport: from solution to device applications

Ritu Gupta,†[a] Anujit Balo,†[b] Rabia Garg,[c] Amit Kumar Mondal,*[c] Koyel Banerjee Ghosh *[b] and Prakash Chandra Mondal *[a]

Received 26th August 2024
Accepted 29th October 2024

DOI: 10.1039/d4sc05736h

rsc.li/chemical-science

The chirality-induced spin selectivity (CISS) effect has garnered significant interest in the field of molecular spintronics due to its potential to create spin-polarized electrons without the need for a magnet. Recent studies devoted to CISS effects in various chiral materials demonstrate exciting prospects for spintronics, chiral recognition, and quantum information applications. Several experimental studies have confirmed the applicability of chiral molecules in spin-filtering properties, influencing spin-polarized electron transport and photoemission. Researchers aim to predict CISS phenomena and apply this concept to practical applications by compiling experimental results. To expand the possibilities of spin manipulation and create new opportunities for spin-based technologies, researchers are diligently exploring different chiral organic and inorganic materials for probing the CISS effect. This ongoing research holds promise for developing novel spin-based technologies and advancing the understanding of the intricate relationship between chirality and electron spin. The review highlights the remarkable experimental and theoretical frameworks related to the CISS effect, its impact on spintronics, and its relevance in other scientific areas.

Introduction

The study of spintronics is an intriguing field that delves into the impact of electron spins in various materials.[1–6] A particularly noteworthy development in spintronic research is the chirality-induced spin selectivity (CISS) effect which was named by Prof. Ron Naaman and David Waldeck and it holds the potential to enable highly effective spin injection into metals or

[a]*Department of Chemistry, Indian Institute of Technology Kanpur, Uttar Pradesh-208016, India. E-mail: pcmondal@iitk.ac.in*

[b]*Department of Chemistry, Indian Institute of Technology Hyderabad, Telangana-502285, India. E-mail: koyel@chy.iith.ac.in*

[c]*Institute of Nano Science and Technology, Knowledge City, Mohali, Punjab-140306, India. E-mail: amit@inst.ac.in*

† R. G. and A. B. equally contributed to this work.

Ritu Gupta

Ritu Gupta obtained her BSc degree in chemistry (Honors) from Sri Venkateshwara College, University of Delhi and her MSc degree in chemistry from the National Institute of Technology, Warangal, in 2019. She received her doctoral degree in 2024 from the Indian Institute of Technology Kanpur, under the supervision of Dr Prakash Chandra Mondal. Currently, she is a post-doctoral researcher at the University of Twente, Netherlands. Her current research focuses on brain-inspired molecular electronics.

Anujit Balo

Anujit Balo is currently working as a PhD scholar in the Department of Chemistry at the Indian Institute of Technology, Hyderabad, India, under the supervision of Dr Koyel Banerjee Ghosh. He received his MSc degree from the Department of Chemistry at Jadavpur University (India) in 2021. His research goals focus on developing chiral molecularly functionalized catalysts for spin-controlled electrocatalysis and their application in metal–air batteries.

semiconductors through chiral materials, without the need for magnetic fields.[7–10] Alternatively, it can be stated that the CISS effect can facilitate the creation of spin-polarized electrons, without the need for a magnet, which could open up new possibilities for spintronics.[11–13] While most spintronic devices are made from (ferro)magnetic materials, the use of chiral organic molecules as spin filters, rather than traditional inorganic materials could enhance energy efficiency and enable device miniaturization. Organic-based spintronic devices are easy to fabricate and can show high spin selectivity that requires a lower magnetic field to switch the spin state from high to low resistance. Back in 1999, Naaman and Waldeck groups first observed the CISS effect using L- or D-stearoyl lysine-based chiral organic films.[14] This phenomenon revealed that photoelectron scattering asymmetry is over 100 times greater when electrons travel through chiral molecules. The CISS effect describes how chiral molecules can selectively transmit electrons with one spin over those with the opposite spin, meaning chiral molecules can act as spin filter.[15–18] Essentially, electrons with specific spins can easily move through chiral molecules in one direction, depending on the handedness of the molecules.[19,20] While there is no complete quantitative explanation for the effect yet, it is thought that the electron moves in a helical electrostatic potential, which may help to explain this phenomenon. As an electron traverses the distinct electrostatic potential of a chiral medium, it experiences a centripetal force perpendicular to its velocity, arising from the curvature of the potential energy landscape created by chiral molecules, which depends on the handedness of the molecule and the corresponding potential. This centripetal force, which confines the electron inside the curved potential, is analogous to a Lorentz force that acts as if it were due to an effective magnetic field (B) directed along the electron's propagation axis (Scheme 1). This effective magnetic field interacts with the electron's magnetic moment inducing a splitting of the electron's spin states, stabilizing one state while destabilizing the other. The chiral

Rabia Garg

Rabia Garg obtained her BSc (Hons) degree in 2021 and M.Sc. (Hons) degree in 2023 from the Chemistry Department at Punjab University, Chandigarh. Currently, she is pursuing her PhD at the Institute of Nano Science and Technology, Mohali, under the supervision of Dr Amit Kumar Mondal. Her research interests include exploring the spin-selective electron transfer process through chiral molecules and investigating the chirality-induced spin selectivity (CISS) effect.

Koyel Banerjee Ghosh

Koyel Banerjee Ghosh received her PhD degree from the Fuel Cell & Battery Division at the CSIR-Central Glass & Ceramic Research Institute, Kolkata (India) in 2017. Later, she worked on molecular spintronics in the Department of Chemical & Biological Physics at the Weizmann Institute of Science, Israel from 2017 to 2021. Since 2022, she has been working as an Assistant Professor in the Department of Chemistry at the Indian Institute of Technology Hyderabad. Her current research interest mainly focuses on advancing spin dependent electrocatalysis in renewable energy conversion and storage.

Amit Kumar Mondal

Amit Kumar Mondal obtained his PhD degree from IISER Bhopal in 2017. He then worked as a postdoctoral fellow at the Weizmann Institute of Science, Israel, and later he moved to the University of Utah, USA, as a postdoctoral research associate. Currently, he is working as a Scientist at INST, Mohali. He has received several prestigious awards and fellowships, including the DST Inspire Faculty Award, RSC's Materials Division Horizon Prize, JSPS and PBC postdoctoral fellowships, and the Raman-Charpak fellowship. His research group is currently focusing on electron spin interactions with chiral materials, exploring the CISS effect and its applications.

Prakash Chandra Mondal

Prakash Chandra Mondal obtained a PhD degree from the University of Delhi. He then moved to the Weizmann Institute of Science, Israel, and worked on spin-dependent electrochemical studies. Later, he worked on molecular electronics at the University of Alberta. Before joining the Department of Chemistry, Indian Institute of Technology (IIT) Kanpur as an assistant professor in 2019, he was a Marie-Curie Post-doctoral Fellow at the University of Valencia, Spain. He is interested in studying molecular electronics and spintronics. He received the P. K. Kelkar Outstanding Young Faculty Research Award in 2024. He is serving as an Analyst board member.

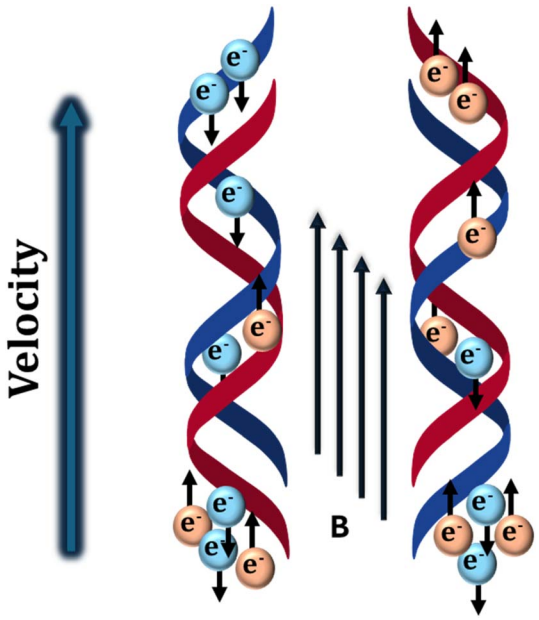

Scheme 1 Schematic representation of the CISS effect where the electron transfer process happens through a chiral potential that facilitates spin-selective electron transmission.

structure thus couples the electron's motion and spin, enhancing the transport of one spin orientation over the other, depending on the handedness of the chiral molecules and the direction of electron motion. This phenomenon establishes a direct relationship between the electron's spin and its trajectory and favors selective spin transport.[21] Moreover, this connection also impedes the backscattering of the electron since reversing the electron's velocity direction necessitates a highly unlikely flip of its spin direction. As a result, the coupling between spin and velocity increases the efficiency of the electron transfer process through chiral materials.

Two primary methods for measuring the CISS effect are analyzing spin-dependent transport through chiral materials or examining the spin polarization induced by charge polarization in chiral materials.[11] To determine the efficiency of the CISS effect, spin polarization (SP) is calculated as $\mathrm{SP} = \frac{(I_{\mathrm{up}} - I_{\mathrm{down}})}{(I_{\mathrm{up}} + I_{\mathrm{down}})}$, where I_{up} and I_{down} correspond to currents of spin-up and spin-down configurations.

This phenomenon has been verified in several chiral materials, DNA and oligopeptides, chiral metal–organic frameworks, amino acids, chiral supramolecules, polymers, proteins, and organic–inorganic hybrid materials.[11,22–24] The CISS effect is relevant in various fields, ranging from spintronics, and enantioselective reactions to chiral recognition and quantum information. Effectively injecting spin has been a challenge with such materials. Fortunately, the CISS effect in organic and inorganic molecules provides a solution. These molecules serve as spin filters by displaying the CISS effect at room temperature, making them highly practical for spintronic applications. Researchers have been thoroughly exploring and refining various organic and inorganic materials to expand the limits of spin manipulation and create exciting prospects for spin-based technologies. Multiple experimental results have been compiled to gather information about CISS phenomena, enabling researchers to construct a knowledge base that predicts the CISS effect and applies it to various applications. This review provides a comprehensive overview of a wide range of materials, including organic, inorganic, and organic–inorganic hybrid systems, utilized in the study of the CISS effect. This review highlights the importance of the CISS effect including significant technological advancements such as magnetoresistance devices, biospintronics, photovoltaics, light-emitting diodes (LEDs), and catalytic processes for the oxygen evolution reaction (OER). By providing both theoretical insights and practical implications, this review presents a more comprehensive and forward-looking perspective compared to others, making it an invaluable resource for researchers in spintronics, materials science, and energy conversion. Additionally, the review delves into advanced experimental techniques such as magneto-conductive atomic force microscopy (mc-AFM), which allows for precise measurement of spin-dependent conductance at the nanoscale, and spin electrochemistry, which examines the interplay between spin polarization and electrochemical processes. By examining a wide array of experimental techniques, the review provides valuable insights into how chiral materials influence spin-dependent processes at the molecular and nanoscale levels, which is crucial for advancing our understanding of spintronics, a field with immense potential for revolutionizing next-generation technologies.

Theoretical frameworks regarding the CISS effect

Although the chirality-induced spin-selectivity effect has been successfully demonstrated in various systems ranging from charge transport in protein molecules to electrocatalysis and magnetoresistance devices, its underlying mechanism still creates some debate among theoreticians. The uncertainty arises from the fact that efficient spin–orbit coupling (SOC) should be responsible for room temperature spin-polarization, which is known to be extremely small in hydrocarbon-based molecules. According to this SOC model, the electron's spinning motion is correlated with its orbital motion in the chiral molecule. To be specific, the electron's spin state is correlated with the molecular chirality that influences its electronic properties. Earlier, it was proposed that this high SOC results from the substrate on which the chiral molecule is adsorbed.[25] Several substrates were investigated to examine the effect although the results were not conclusive enough.[26] Later, some experimental results demonstrated that this effect has weak temperature dependence for electron transfer. Michaeli *et al.* suggested a temperature-independent mechanism, in which an electric potential builds up across the molecule. It was found to be extremely worthy in explaining the electron transfer across an appreciable distance even at zero temperature.[27] According to this theory, upon application of a potential across the chiral molecules (known as

chiral potential), the nature of the energy states of the molecule changes from being confined. Hence, efficient resonant tunneling over a longer distance becomes possible without any thermal activation. However, later Fransson *et al.* reported that CISS is correlated with temperature.[28] He proposed a model for a chiral molecular system mounted between metallic leads. According to this model, spin-dependent electron–phonon coupling originates from spin–orbit interactions, and it leads to exchange splitting between the spin channels in the structure. This model fits very well with the experimental data obtained at room temperature. Later, Das *et al.* measured the magnetoresistance of chiral oligopeptide monolayers adsorbed on the ferromagnetic substrate.[29] The measurements were carried out by varying the angle between the magnetization of the ferromagnet and the surface normal as a function of temperature and this was carried out for both the enantiomers. The angle dependence was found to exhibit a varying trend with a periodicity of 360°. This observation was also explained by significant spin–orbit coupling (SOC), which includes the contribution from vibrations. The simulation can replicate the experimental results only if electron–phonon interactions and dissipation are included.

Chiral organic materials for spintronics

Organic materials are attractive for spintronics because of their small spin–orbit coupling, which allows for long-range spin coherence over longer times and distances than conventional inorganic heavy materials. However, organic molecules are typically not a good choice for spin injection because of their small spin–orbit coupling. The CISS effect is a promising development for chiral organic spintronics, as chiral molecules can transmit a preferred spin through specific handedness when charge carriers are created. For instance, Kiran *et al.* reported that enantiopure helicene molecules oriented on a graphite surface act as efficient spin filters.[30] Helicenes are fully conjugated carbon rings that lack stereogenic carbons. Due to the repulsion between their termini, helicenes adopt permanent helical conformations that can be either left-handed or right-handed. The authors employed magnetic conductive probe atomic force microscopy (mc-AFM) in two distinct configurations to study the role of spin in the electron transport process through molecular films. The results have significant consequences for understanding the fundamental principles of spin-dependent transport in molecular systems, which have been further employed to design CISS-based electronic devices. The percentage of spin polarization (SP) was found to be +49% $\pm$ 3% and −45% $\pm$ 3% for *P* and *M*-enantiomers, respectively, at $\pm$1.0 V. Kettner *et al.* showed that various helicenes can exhibit spin selectivity.[26] Safari *et al.* demonstrated the first observation of the CISS effect through single chiral heptahelicene molecules (Fig. 1).[31] The authors measured the CISS effect through heptahelicene molecules sublimed *in vacuo* onto ferromagnetic cobalt surfaces. The examination was carried out using spin-polarized scanning tunneling microscopy (SP-STM) at 5 K. The results revealed magneto chiral conductance asymmetries of up to 50% at 5 K. The study introduces a novel approach for analyzing single molecules, representing a significant advancement over previous studies in the field. The approach permits the differentiation of handedness among molecules with a given magnetization. This key discriminator provides a means to compare the conductance of enantiomers. The ability to compare enantiomer conductance in this manner is expected to provide valuable insights into molecular-level electronic properties and CISS mechanisms. Notably, the measurement was performed at a temperature of 5 K. The measured values are akin to those obtained at room temperature for cationic helicenes using the mc-AFM technique and a magnetic Ni-tip. The comparison of conductance asymmetry and polarization of different molecular substrates poses a significant challenge for this approach. Suda *et al.* reported a ground-breaking discovery related to the spin selectivity of chiral molecules that can be changed by external stimuli like temperature or light using an artificial molecular motor made of overcrowded alkenes (OCAs) (Fig. 2).[32] A magnetoresistance (MR) device was fabricated which could validate the observation of spin-polarized current. Despite this, the device yielded an insignificant MR value of approximately 2% due to unpolarized leakage currents. To better estimate the SP values, the mc-AFM technique was further utilized. The thin films were made *via* spin-coating onto the HOPG substrate, followed by current–voltage (*I*–*V*) measurements using CoCr-based AFM tips (Fig. 2). The magnetization was oriented in either an upward or downward direction. At least 40 *I*–*V* curves were collected for each magnetized direction, and their average was calculated. Irrespective of the molecular chirality, there is always a higher absolute current under a positive bias. This is attributed to the variation in work function between the HOPG substrate and the CoCr tip. The motor showed spin selectivity values of up to 44%.

Another study by Zhu *et al.* found that first-generation molecular motors exhibit multistate switching of spin selectivity.[33] There are four chiral states in which these compounds exist, which can be accessed through external stimuli like light and heat. Raman spectroscopy reveals that the molecular motors undergo isomerization when deposited on gold substrates, triggered by exposure to light and heat. This exceptional system can be interconverted in a specific arrangement, either clockwise or counterclockwise. The mc-AFM measurements confirmed the ability of molecular motors to act as spin filters. The irradiated samples underwent successful conversion, predominantly yielding diastereoisomers despite a moderate proportion of metastable to stable isomers. This highlights the significant importance of the spin-polarization in the mentioned studies. The study also showed that the right-handed motor in the photostationary state exhibits efficient spin polarization, with the modulation of spin filtering properties achieved by regulating the sequence of helical states.

Other than this, biomolecules, including DNA, oligopeptides, and proteins such as cytochromes and bacteriorhodopsin, have been incorporated into CISS effect studies due to their preferred handedness.[34,35] Recently, Gupta *et al.* fabricated a soft biomolecular junction using a classical 'flip-chip' approach, where *Ustilago maydis* Rvb2 protein, an ATP-dependent DNA helicase, was sandwiched between two conducting

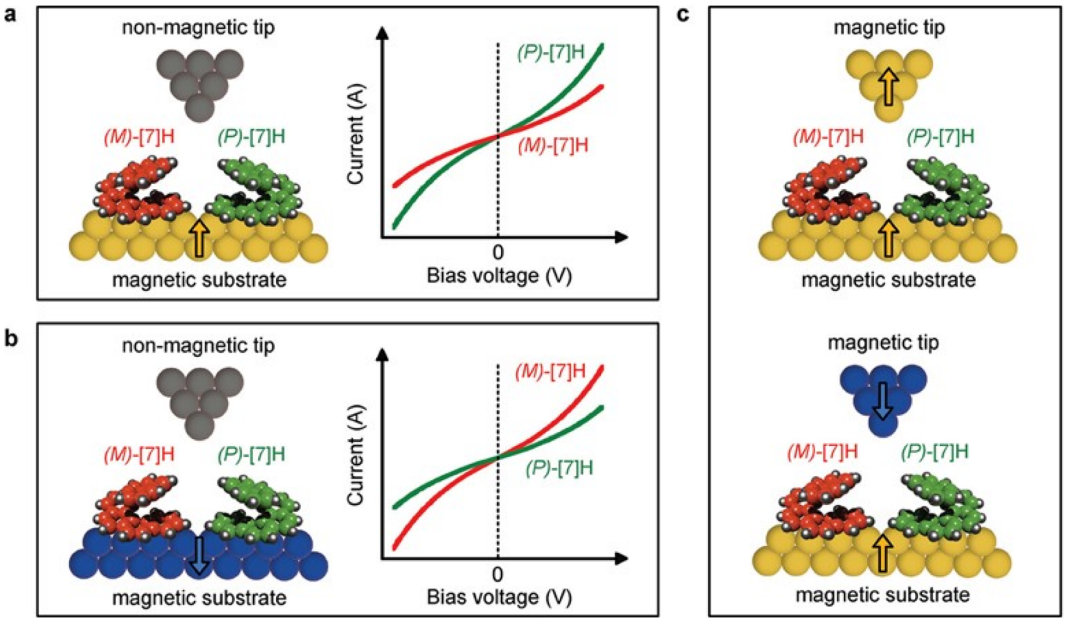

Fig. 1 (a and b) Demonstrating the magneto-chiral electron tunneling on the ferromagnetic electrode for heptahelicene enantiomers. (c) Measurements of STM conductance with a magnetic STM tip on a ferromagnetic substrate. Figures are adapted with permission from ref. 31 (copyright 2023, Wiley).

substrates: ferromagnetic Ni and indium tin oxide (ITO).[36] In the present study, the authors utilized the novel *Ustilago maydis* Rvb2 protein; its hexameric and helical structures along with room temperature stability made it suitable for CISS studies. The Ni substrates were covalently modified with a glutathione (GSH) linker to electrostatically bind the Rvb2 protein, and the junction was completed by using a PMMA gel-coated ITO electrode as the top electrode, as shown in Fig. 3a. The authors employed a different approach compared to many other protein-based electrical junctions. The gel electrolyte protects the underlying protein layers. Interestingly, all devices were fabricated without using any expensive cleanroom facility for vacuum top-electrode deposition. The vacuum-deposited top electrode on the protein film can often denature the protein film and, hence, reduce the device's performance. Thus, the current work illustrates a versatile and facile approach for creating a stable mechanical contact underneath the Rvb2 protein film.

In comparison to the DOWN-magnet and no-magnet conditions, the biomolecular junction demonstrated higher current density and differential conductance under the UP-magnet condition, an evident signature of the CISS effect (Fig. 3b–d). More importantly, the Rvb2 protein-based junctions demonstrated a 30% spin-polarization at 500 mV bias at room temperature, even with a thicker film of $\sim$266 $\pm$ 12 nm (Fig. 3e). Both the asymmetric density of states of Ni substrates at the Fermi energy level and the spin-filtering nature of the Rvb2 protein due to its preferred handedness contributed to the long-range spin-selective charge transport in the biomolecular junction (Fig. 4). The covalent interface between the ferromagnetic Ni substrate and GSH further assisted in enhancing the spin diffusion length without spin decoherence. Thus, this work demonstrates the room-temperature operation of a spintronic device, which is a prerequisite for commercialization.

Chirality plays a vital role in spin filtering in various organic polymers and π-conjugated molecules. The chiral polymers and supramolecular structures are a great alternative for achieving high spin selectivity due to the CISS effect. For example, Mondal *et al.* reported that cysteine–thiophene-based polymers exhibit strong spin filtering properties.[37] It has been shown that spin-selective transport in supramolecular structures holds critical significance.[38] This was accomplished using a helical chiral structure, which facilitated the intended process through the CISS effect. A recent study conducted by Kulkarni and co-workers using a helical supramolecular outweighs the presence of chiral centers in a supramolecular structure.[39] To illustrate this finding, researchers utilized coronene bisimide-based organic molecules with chiral alkoxyphenyl side chains to form nanofiber structures. These fibers were transferred onto a magnetized nickel–gold surface, with the magnetization oriented perpendicular to the surface plane. The AFM tip was set at ground potential and a different bias was applied to the substrate. Nanofibers are bundled due to π-stacked aggregation, resulting in a thickness of 17 $\pm$ 3 nm (Fig. 5).

The spin filtering efficiency was consistently more than 80% at room temperature with thicknesses ranging from 10 to 40 nm. Furthermore, the weak dependence on thickness suggests that obtaining high polarization values for thinner nanofibers is an effective means of ensuring the maintenance of these values even for thicker ones. Based on these findings, it can be established that the magnitude of spin polarization (SP) in this range of heights is reliably high and persistent, which has important implications for future research in this area. It was also demonstrated that SP values can be further manipulated by

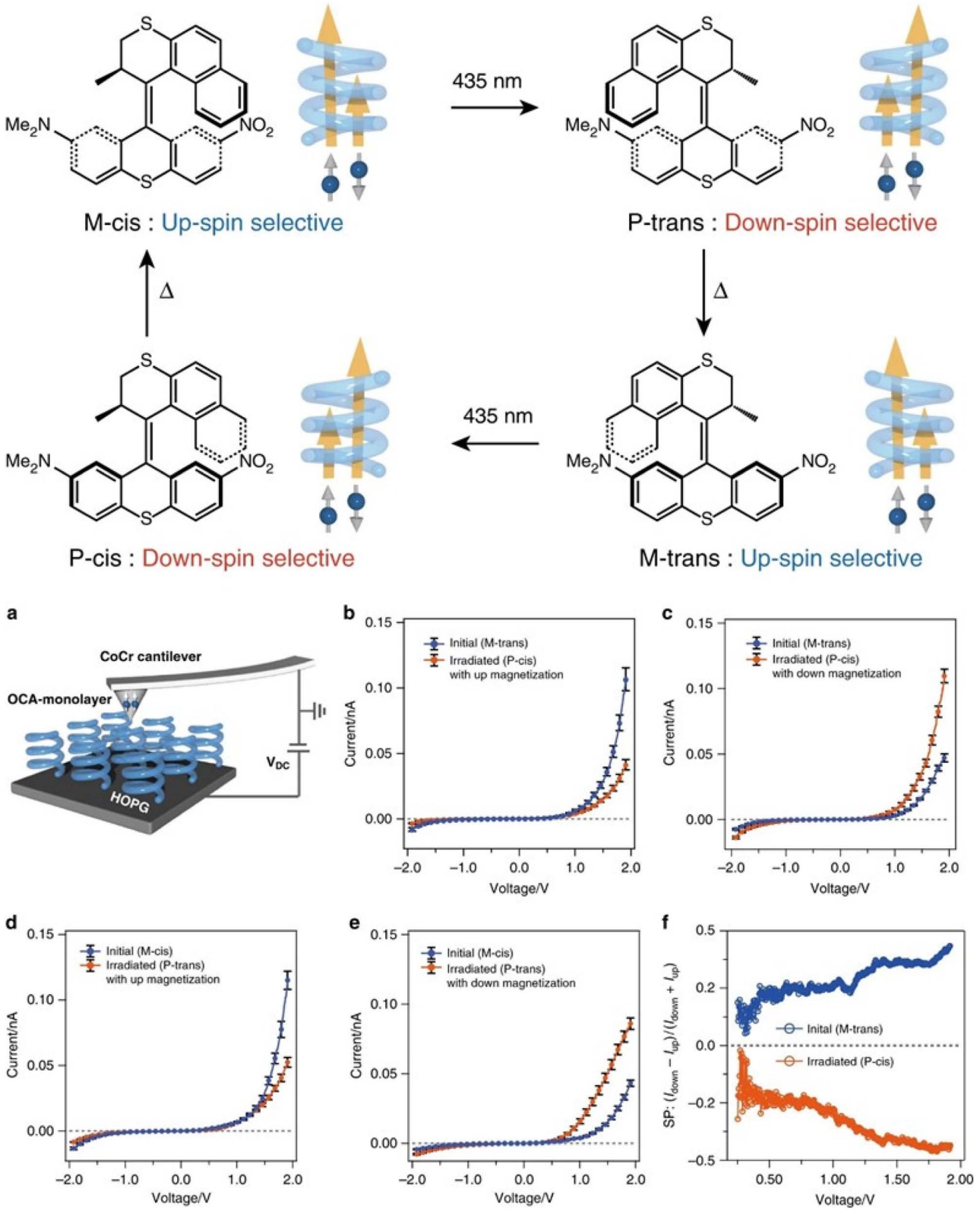

Fig. 2 Molecular structures and rotation cycles of an artificial molecular motor of overcrowded alkenes. (a) Schematic representation of mc-AFM measurements. Representations of *I*–*V* plots for *M-trans* isomers before and after irradiation with the tip magnetized in upward (b) and downward (c) magnetic field orientations. Representations of *I*–*V* plots for *M-cis* isomers before and after irradiation with the tip magnetized in upward (d) and downward (e) magnetic field orientations. (f) Plot of spin polarization *vs.* applied voltage before and after the irradiation. Figures are adapted with permission from ref. 32 (copyright 2019, Nature).

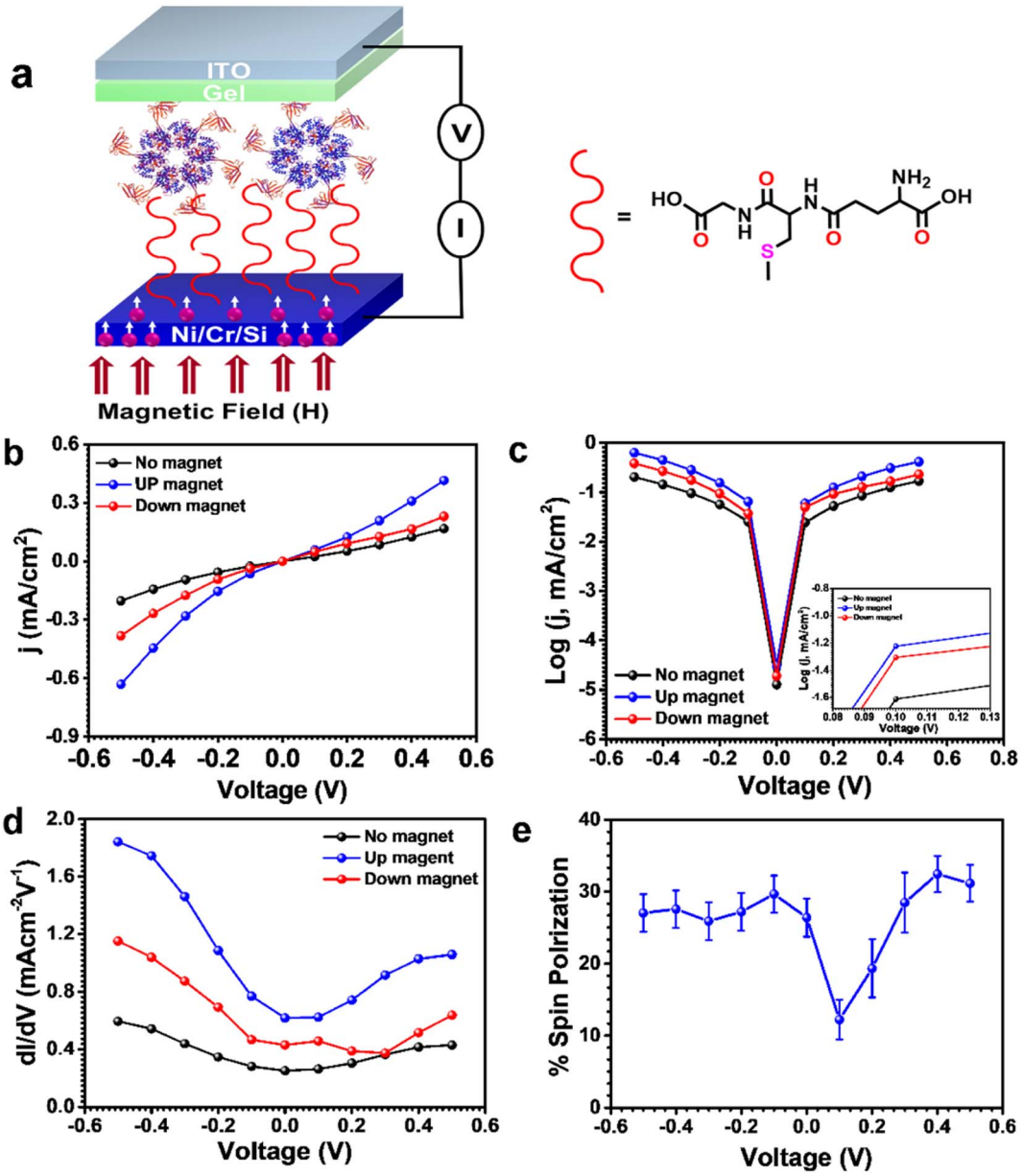

Fig. 3 Spin-selective charge transport in Rvb2-based biomolecular junctions. (a) Schematic illustration of the Ni/Rvb2/ITO biomolecular junction. (b) j–V curves, (c) semilog curves and (d) derivative conductance curves of Ni/Rvb2/ITO biomolecular junctions in the absence and presence of an applied magnetic field. (e) Spin polarization as a function of applied bias. Figures are adapted with permission from ref. 36 (copyright 2023, American Institute of Physics).

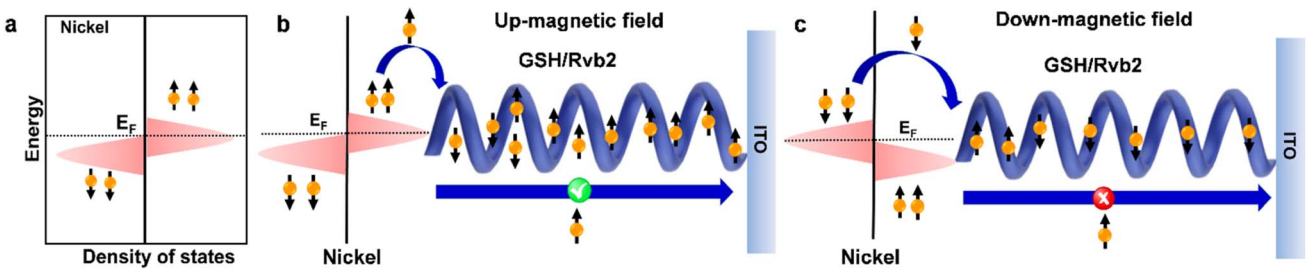

Fig. 4 Mechanistic model for spin-selective charge transport in Rvb2-based junctions. (a) Energy *vs.* density of states plot for the ferromagnetic Ni substrate in the absence of an applied magnetic field. (b and c) Proposed spin-selective charge transport in Ni/Rvb2/ITO junctions under spin-UP and spin-DOWN magnetic field conditions. Figures are adapted with permission from ref. 36 (copyright 2023, American Institute of Physics).

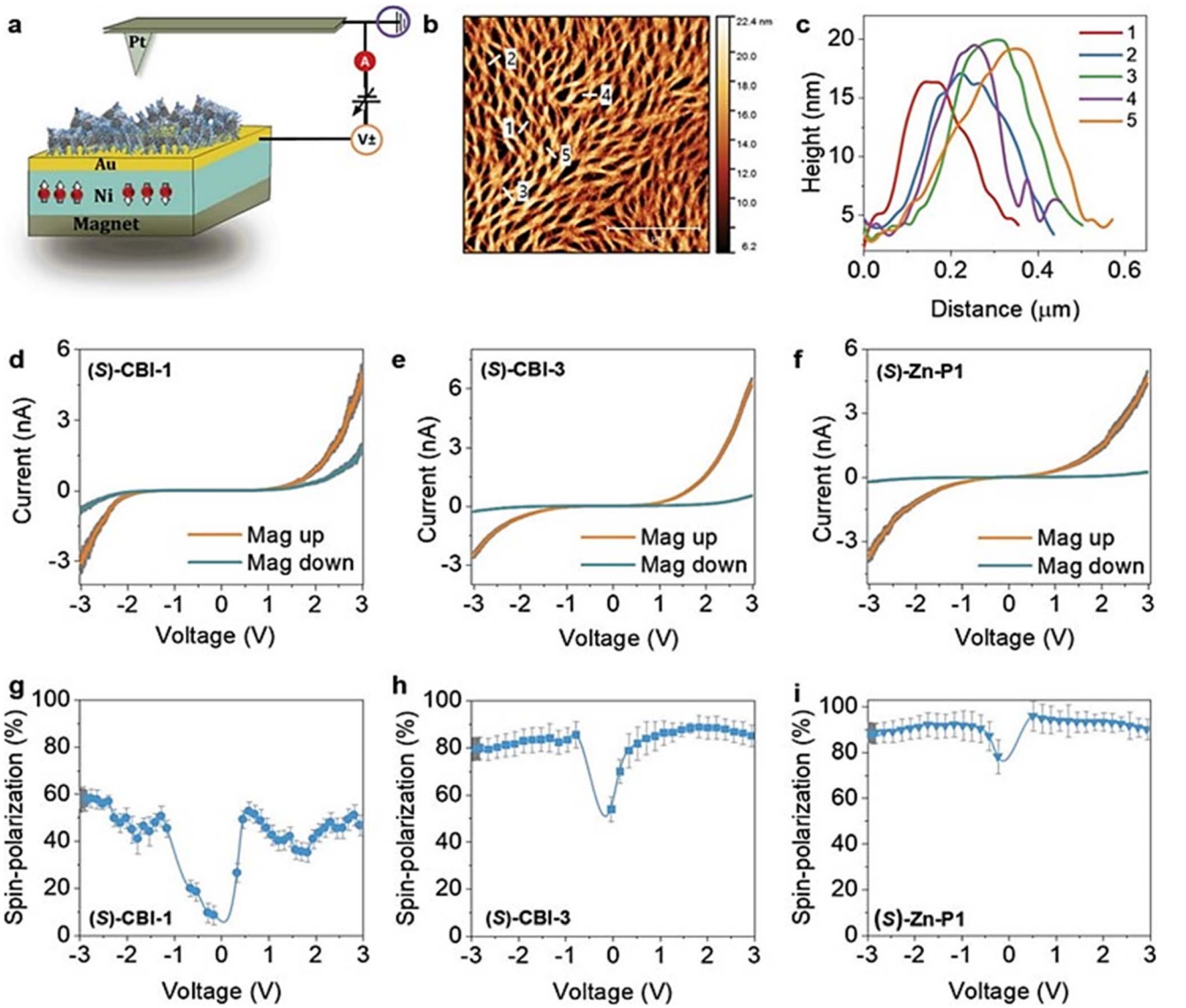

Fig. 5 (a) Representation of the mc-AFM setup. (b and c) AFM image of the supramolecular nanofibers and AFM height profiles. (d–f) The averaged *I–V* plots for different samples showing the Ni film magnetized with the north pole pointing up (orange) or down (cyan). (g–i) The plot of SP% *vs.* voltage for different samples. Figures are adapted with permission from ref. 39 (copyright 2020, Wiley).

mixing the chiral and achiral assemblies through the chiral amplification effect. The authors reported a strong correlation between the molecular structure and the spin-filtering efficiency (Fig. 6). Typically, the supramolecular helicity changes based on the stereoconfiguration of the chiral centers in the molecules; however, the study showed that the same L-chirality of the molecule can also produce left and right-handed helicity and that the spin filtering property can be inverted by changing the temperature (Fig. 6).

Earlier studies for understanding the CISS effect at the molecular level, however, did not consider the impact of the polymer backbone on the spin-filtering property. To address this issue, Mishra *et al.* reported the CISS effect in which spin-polarized electrons are transferred along the primary molecular axis of the polymer backbone.[40] The authors used thiol (–SH) functionalized poly(phenylacetylene)s that were self-assembled on the gold surface. The spin polarization was approximately 53% and 56%, resulting in a spin transmission ratio of approximately 1 : 3 (Fig. 7). Interestingly, there was no discernible difference in the averaged *I–V* plots for optically inactive polymer samples in the presence of different magnetic field orientations. Earlier CISS-based mc-AFM measurements indicated a non-linear current–voltage relationship. The two spins exhibited distinct thresholds for charge injection, indicating that no spin-flipping process was involved. The spin injected at a lower potential depends on the chirality of polymer samples, with a difference in the injection threshold of roughly 100 : 10 meV (Fig. 7). For the D-polymer, the lower spin corresponds to the magnet pointing down, which means that the injected spins are polarized parallel to the electron's velocity. To investigate the feasibility of these polymers for spintronics applications, a spin valve device was fabricated, and the

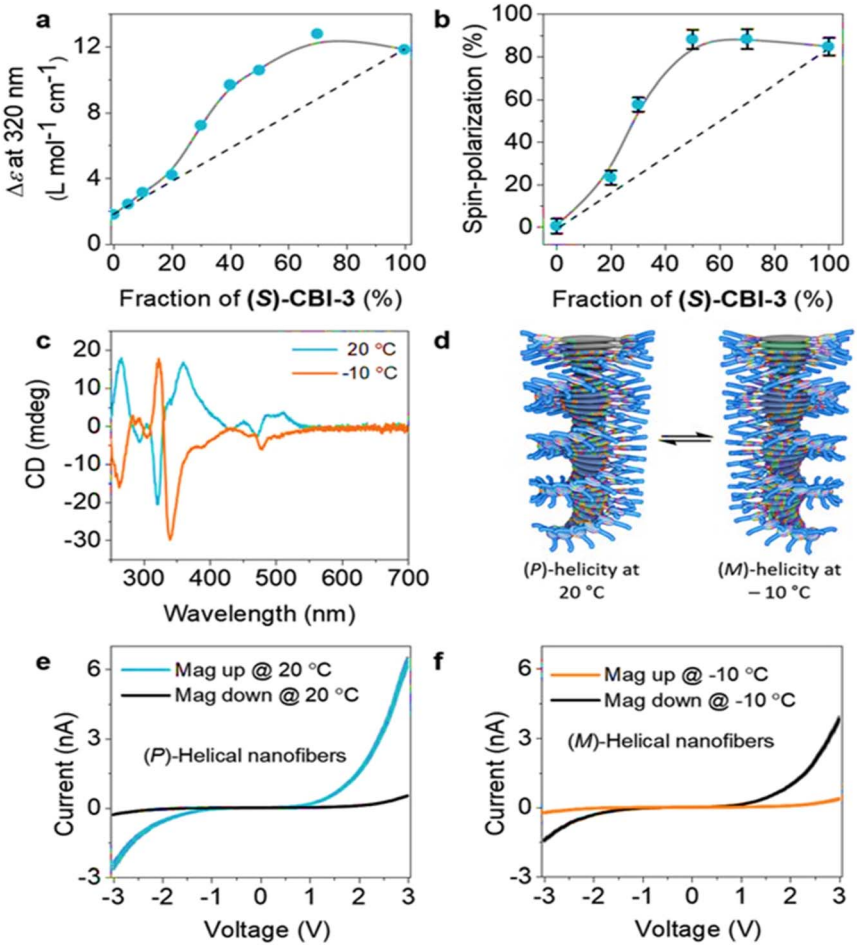

Fig. 6 (a) Plot of molar circular dichroism ($\Delta\varepsilon$) *vs.* fraction of chiral molecules. (b) Spin polarization values at +3 V for different fractions of samples measured by mc-AFM. (c) Temperature-dependent CD plots. (d) Schematic representation of helical chirality depending on different temperatures. (e and f) The averaged *I*–*V* plots for chiral samples at different temperatures. Figures are adapted with permission from ref. 39 (copyright 2020, Wiley).

magnetoresistance (MR) effect was subsequently measured. Unlike other MR devices, the MR behavior of this device exhibited asymmetry relative to the field sign (Fig. 7), which is attributed to the use of one ferromagnetic electrode. The MR values are relatively low likely due to the presence of pinholes in the monolayers and electron scattering.

Previous studies have observed spin-selective transport in supramolecular structures that use homochiral building blocks with stereocenters. One may question whether the presence of stereocenters is crucial for observing the CISS effect. This is a pivotal point for consideration, as it could greatly impact our understanding of this phenomenon. A recent report by Mondal *et al.* demonstrated that the spin selectivity arises not from individual stereocenters of supramolecular structures but rather originates from helical supramolecular nanofibers.[41] The authors successfully demonstrated that the CISS effect originates from supramolecular structures having only achiral monomers. They employed triphenylene-2,4,10-tricarboxamide motifs that possess helical chirality to investigate the spin polarization of the samples (Fig. 8). The helical chirality was deliberately manipulated to selectively produce opposite helices through the application of chiral solvents. The results indicate that the SP values increased with the sample's thickness, and the effect was found to be non-local, as evidenced by the intensity of the CD signals of the polymers. The thickness dependence can be attributed to at least two mechanisms operating, namely, the CISS effect and the scattering process. Moreover, the temperature dependence supports that phonons may contribute to the CISS effect.

The recent work by Rösch *et al.* demonstrated a significant contribution of helical order to the CISS effect at chiral centers using squarine dyes.[42] The efficient spin filtering ability is mainly due to the chiral molecules that are typically organized through anchoring groups or supramolecular polymers. Recently, Labella *et al.* reported a new type of spin-filtering material based on bowl-shaped subphthalocyanine-based molecules, and the spin polarization was nearly 50%.[43] From the *I*–*V* characteristics, it is clear that the magnetization direction of the substrate is a crucial factor in determining the current exhibited by both the enantiomers. Precisely, the *M*-enantiomer shows higher currents when the substrate is magnetized with the magnetic field oriented upward.

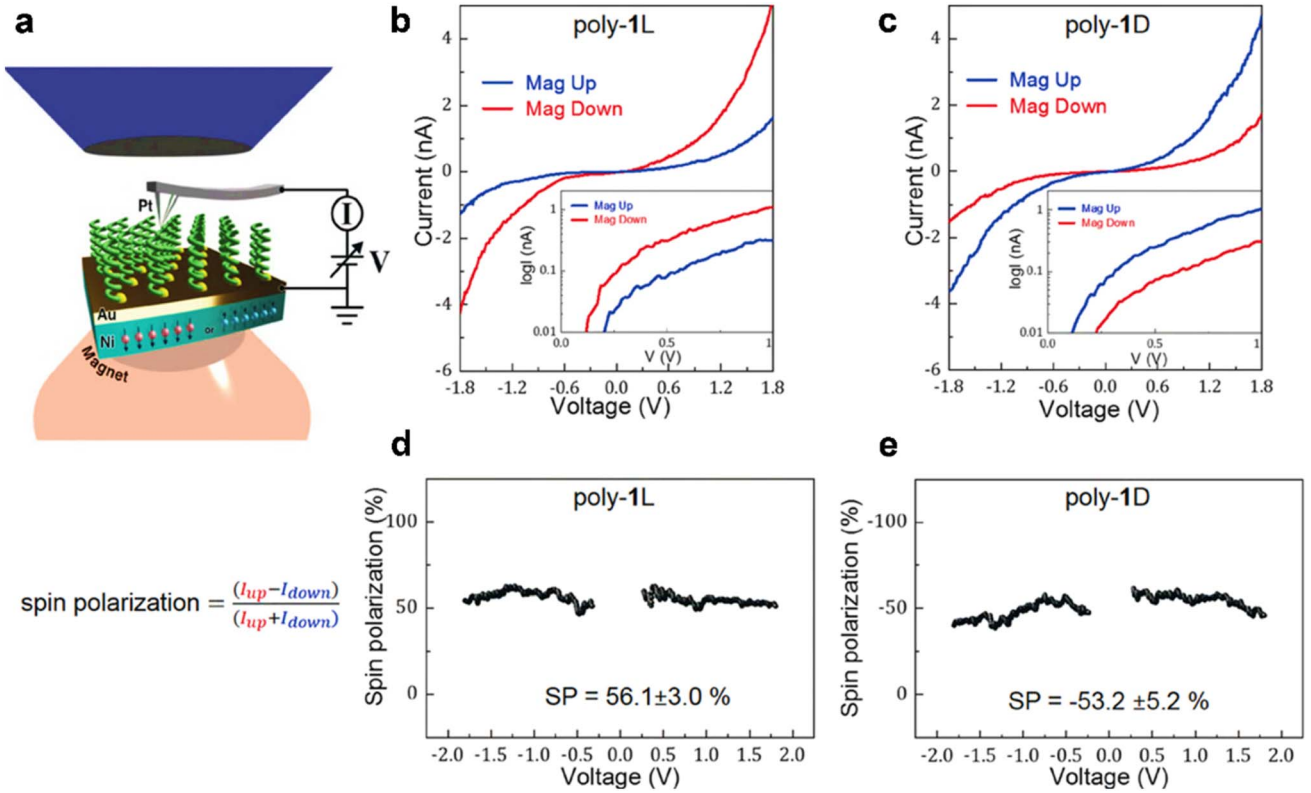

Fig. 7 (a) Scheme of the mc-AFM setup. (b and c) Averaged *I*–*V* plots for L and D polymers, respectively. (d and e) The spin polarization *vs.* voltage plots for L and D polymers, respectively. Figures are adapted with permission from ref. 40 (copyright 2020, Wiley).

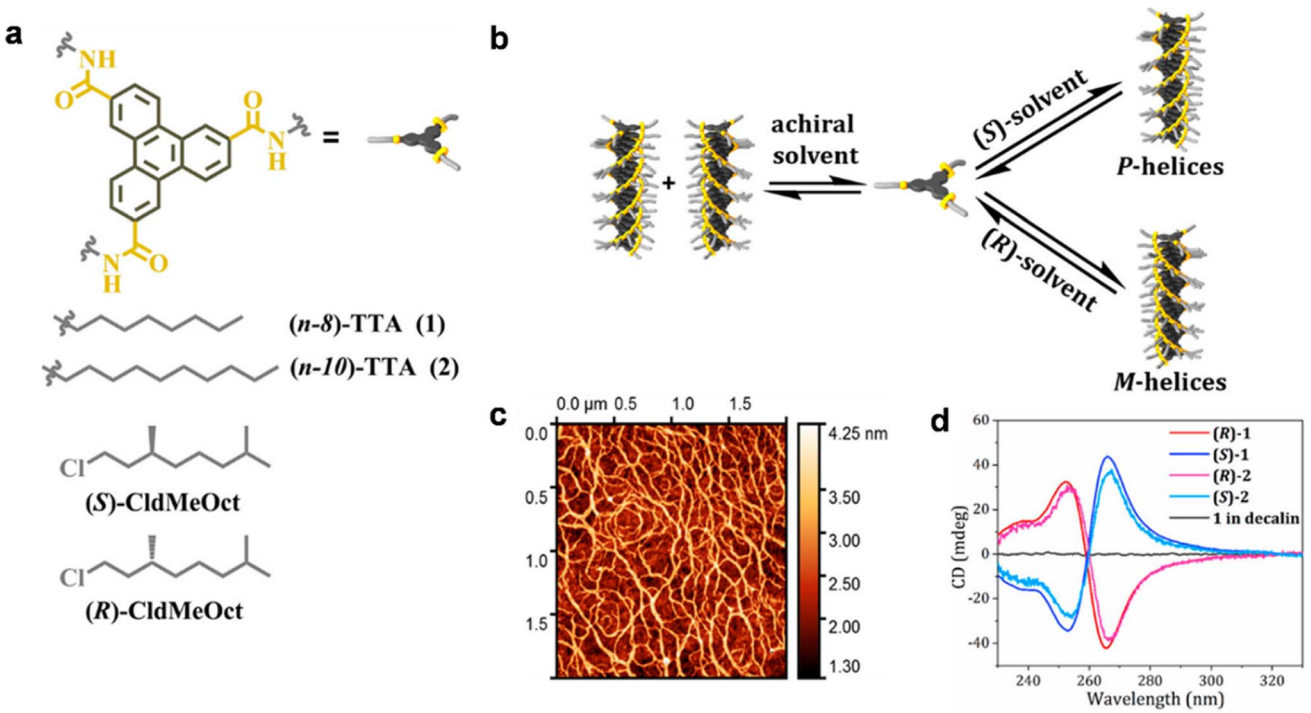

Fig. 8 (a) Chemical structures of achiral molecules and chiral solvents. (b) Representation of chiral self-assembly processes involving solvent molecules. (c) AFM image of the nanofibers. (d) CD spectra of molecules made from chiral (*S*)-and (*R*)-solvents. Figures are adapted with permission from ref. 41 (copyright 2021, American Chemical Society).

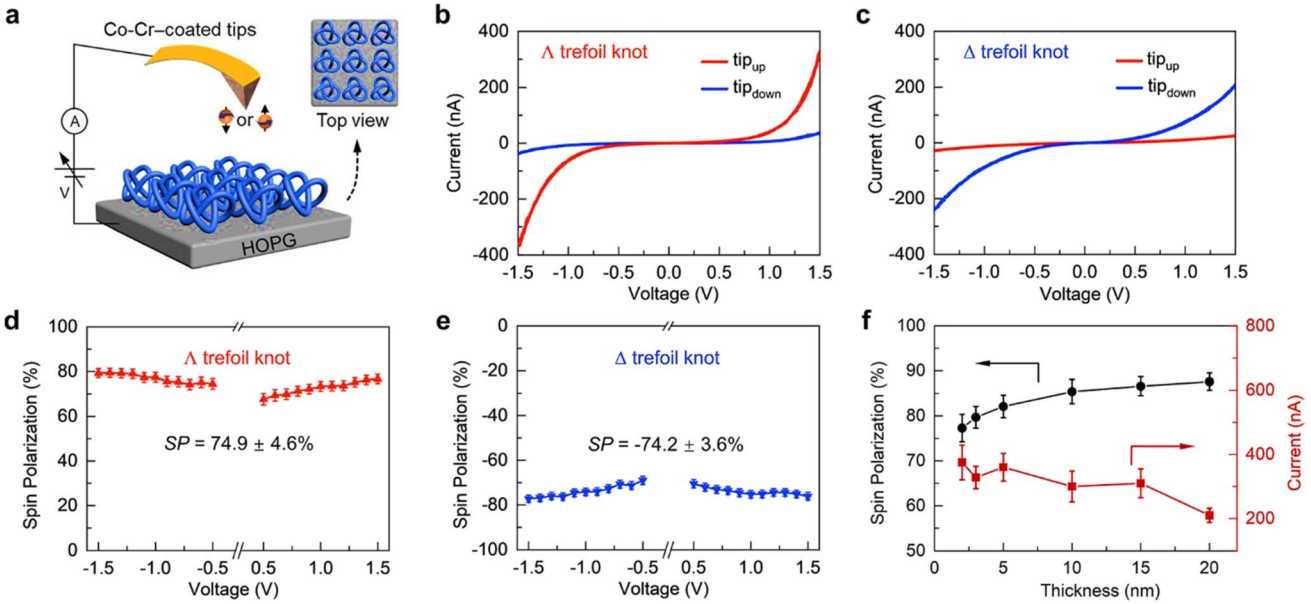

Fig. 9 (a) Representation of the mc-AFM setup. The averaged *I*–*V* plots for Λ (b) and Δ (c) molecular trefoil knots. The plot of spin polarization *vs.* applied voltages for Λ (d) and Δ (e) knots. (f) Thickness-dependent SP% values and current intensities. Figures are adapted with permission from ref. 45 (copyright 2023, American Chemical Society).

Conversely, the current is lower in the case of the *P*-enantiomer when the same magnetization is applied. Notably, the spin polarization values are relatively high, despite the absence of any anchoring groups or supramolecular polymerization. This underscores the remarkable self-organizing ability of subphthalocyanines in thin films. These promising findings suggest that bowl-shaped aromatic molecules could offer practical and effective materials for CISS-based spintronic devices.

Giaconi *et al.* have recently demonstrated the high spin selectivity of above 60% in self-assembled monolayers of thia[4]heterohelicenes prepared on a gold electrode.[44] From mc-AFM measurements, it has been found that spin-selective electron transport occurs at low voltages of ±0.3 V. Zhang *et al.* very recently reported that topologically chiral knot molecules despite the absence of stereogenic atoms behave as a new type of spin-filtering material at room temperature (Fig. 9).[45] The intrinsic chirality has been confirmed from CD spectra and correlated with a very high spin polarization of up to 88% as evident from mc-AFM measurements. The Λ trefoil knot exhibited higher current levels when the tip was magnetized upwards, while the Δ trefoil knot displayed the opposite trend, with higher current recorded when the tip was magnetized downwards.

In a controlled experiment, the samples containing a 50/50 mixture of Λ and Δ trefoil knots were tested, and no discernible difference was observed under the two different magnetic field directions. The spin polarizations for the Λ and Δ molecular trefoil knots were calculated to be 74.9 ± 4.6% and −74.2 ± 3.6%, respectively. Accordingly, the chiral knots provide a viable opportunity for the advancement of a novel class of spintronic elements. This innovative approach holds significant promise for advancing the field of organic spintronics, given the unique properties of chiral knot molecules.

Organic–inorganic hybrid materials for CISS-based spintronics

The employment of inorganic–organic hybrid materials in various relevant applications reveals their potential as promising materials for use as spin filters. It has been demonstrated that the functionalization of inorganic materials with chiral organic molecules results in spin-polarization in the hybrid materials at ambient temperature. Besides, by utilizing various types of organic molecules, long-range spin-selective electron conduction through inorganic–organic hybrid materials is possible. To discuss the exploration of different chiral inorganic–organic hybrid materials in detail, this section is divided into the following sub-sections.

Magnetoresistance devices

The importance of inorganic–organic hybrid materials in the fields of photovoltaic,[46] optoelectronic, and electrochemical devices is well documented. In recent years, its relevant application in the field of spintronics have also been demonstrated. There are many reports demonstrating the conduction of spin-selective electrons through organic–inorganic hybrid systems using ferromagnetic (FM) materials.[47] It has been found that a spin-valve consisting of two colossal magnetoresistance (CMR) half metallic electrodes and an organic semiconductor (Fig. 10) situated between them results in large magnetoresistance for channel lengths of the device less than 140 nm whereas magnetoresistance is absent for longer channel

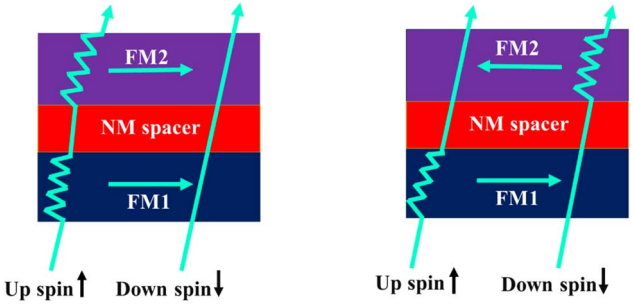

Fig. 10 Schematic representation of a spin-valve structure demonstrating spin-dependent scattering at the two ferromagnetic electrodes in both parallel and antiparallel alignments as shown in the literature. The figure is reconstructed from ref. 47.

lengths. This observation supports the notion that spin-polarized transport occurs through the organic semiconductor. Carrier injection probability for shorter channel length is proportional to the acceptance probability by the second ferromagnetic electrode. Thus, the resistance for parallelly oriented electrodes with the same spin alignment decreases and is responsible for the magnetoresistance signal. The spin polarisation is missing for longer channel lengths *i.e.*, for longer organic semiconductors.

Spin injection into the organic material and coherent spin transport through it, are considered two processes involved in the spin polarization effect.[48] A significant enhancement in the spin transport efficiency has been reported by employing an n-type semiconducting polymer P(NDI2OD-T2) as the nonmagnetic spacer in spin valves by Li *et al.*[49] This indicates that exceptionally high magnetoresistance can be achieved at room temperature by improving the semiconducting polymer and Co FM electrode interface by introducing a thin layer of AlO_x as well as optimal annealing of the bottom $La_{2/3}Sr_{1/3}MnO_3$ (LSMO) electrode. Furthermore, it has also been found that transport through the polymeric interlayer is spin-dependent and the spin diffusion length shows weak dependence on the temperature.[49] After the invention of the CISS effect, numerous organic–inorganic hybrid materials have been explored for spin-selective electron transfer. As demonstrated by Bloom and others, CdSe quantum dots functionalized with chiral cysteine molecules allow spin-selective electron transfer (Fig. 11), which was investigated using magnetic conductive-probe atomic force microscopy (mCP-AFM) measurements as well as magnetoresistance measurements.[50] It is also shown that chirality-modified metal–organic crystals (MOCs), *e.g.*, Cu(II) or Co(II) phenylalanine enable long-range, spin-selective electron conduction at ambient temperature.[51,52] The metal ions are organized in two-dimensional layers between either L- or D-enantiomers of pentafluorophenylalanine (F_5Phe) or phenylalanine (Phe).

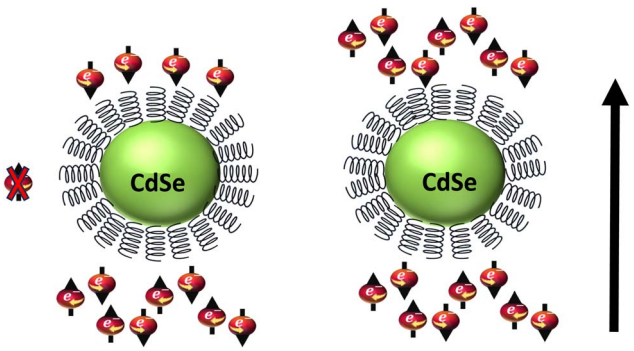

Fig. 11 Schematic representation illustrating charge conduction *via* cysteine functionalized CdSe quantum dots with spin selectivity.

The studies of spin-selective electron conduction through chiral enantiomer performed by mCP-AFM have revealed higher current for L-enantiomers of phenylalanine with up-spin magnetization while the opposite behavior has been observed for D-enantiomers (Fig. 12). It has been proposed that the preferred spin injection depends on handedness (L or D) while the preferred spin transport depends on the magnetization direction of the molecular ferromagnet, which is independent of chirality. So, different current magnitudes for L- and D-enantiomers with up and down spin magnetized substrates have been observed. The unusual thermally activated ferromagnetic behavior observed in this Cu-phenylalanine crystal can be explained by an indirect interaction between the unpaired electrons on the Cu(II) ion, which is mediated through the chiral lattice, forming a low-lying thermally populated ferromagnetic state while the Co-phenylalanine crystal shows antiferromagnetic interaction due to slight changes in its crystal structure. These studies highlight the combined effect of paramagnetic ions and the chiral lattice, expanding their relevance to the organic molecule-based spintronics applications.

Photovoltaic & light emitting diodes

The spin-filtering property of chiral molecules offers great opportunities in photoinduced spintronics applications. After the invention of the CISS effect, several studies have demonstrated that chiral molecular assemblies exhibit spin-polarization at room temperature. Spin polarization has been achieved by utilizing photoinduced charge separation and injection from well-coupled organic chromophores or quantum dots like CdSe at room temperature.[53] Exploiting the CISS effect, the organic bulk heterojunction's photoconversion efficiencies can be improved by spin-selective charge transport. Zhang and others explored how the reduction of the recombination of polaron pairs at the interface of poly(3-hexylthiophene/1-(3-(methoxycarbomyl)propyl)-1-1-phenyl)(6,6) C_{61} (P3HT-PCBM) can be achieved by doping with spin-polarized galvinoxyl radicals, which results in an efficiency increase by 18%.[54] They proposed a spin-flipping mechanism that suggests an exchange interaction between spin-polarized radicals and charge acceptors resulting in the suppression of the polaron pairs recombination rate by converting their spin from the singlet to the triplet state (Fig. 13a). Giovanni and others highlighted low-temperature solution-processed organic–inorganic hybrid halide perovskite CH_3NH_3PbI, as a promising candidate due to its ultrafast spin-switching

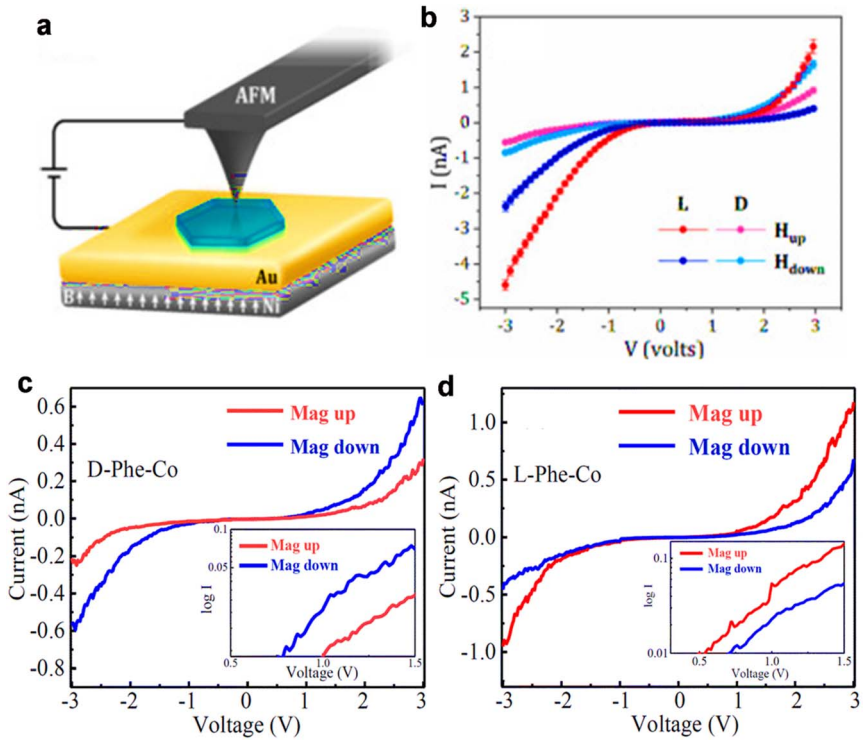

Fig. 12 Spin-selective conduction. (a) Schematic representation of the mCP-AFM measurement. The catalyst is coated on a gold coated Ni surface and a conducting AFM tip is in contact from above. An external magnetic field is used to magnetize the substrate. The current–voltage (*I*–*V*) measurements plots of (b) D- and L-Phe-Cu crystals magnetizing the substrate with different magnetic orientations. (c and d) The current–voltage (*I*–*V*) measurement plots of D- and L-Phe-Co crystals measured at room temperature. The log *I*–*V* plot is shown in the insets in (c) and (d). Figures (a and b) are adapted with permission from ref. 51 and figures (c and d) are adapted with permission from ref. 52.

capability in photovoltaics and light-emitting devices, despite its large spin–orbit coupling and small spin electron–hole relaxation lifetime.[55–57] It has been observed that chiral semiconductor-based quantum dot thin films can preferentially transmit a particular spin-oriented electron. Recently Das *et al.* reported chiral $(R\text{-}/S\text{-MBA})_2CuCl_{4-x}Br_x$ compounds with tunable band gaps for photovoltaic and photocatalytic applications.[58]

It has been revealed that the lack of spin-polarized charge carriers in semiconductors at room temperature limits their application in opto-spintronics. A hybrid inorganic/organic spin light-emitting diode (h-OLED) has also been found to produce ~80% giant magneto-electroluminescence with the emission of red, green, and blue lights.[59] Recently it has been demonstrated that spin-polarized charge carriers can be injected into hybrid organic–inorganic trihalide perovskites, namely

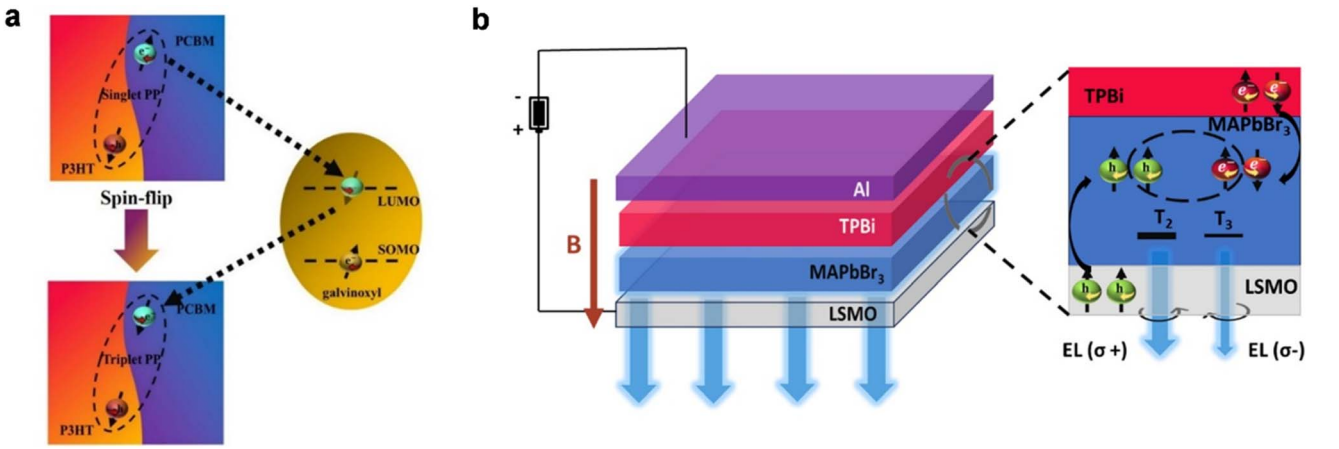

Fig. 13 (a). Schematic representation of the spin-flipping mechanism *via* galvinoxyl radicals. (b). Schematic representation of the spin-LED device architecture consisting of a half-metal LSMO anode, $MAPbBr_3$ light emitting layer, and TPBi molecule thin film as the electron transport layer covered with an Al cathode. Figure (a) is reconstructed from ref. 54. Figure (b) is adapted with permission from ref. 60.

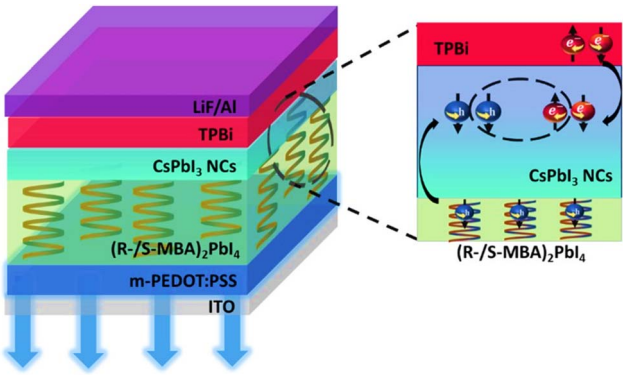

Fig. 14 Schematic representation, illustrating the spin-polarized charge injection and circularly polarised electroluminescence emission in spin-LEDs as demonstrated in the literature. The figure is reconstructed from ref. 62.

methylammonium lead bromide ($MAPbBr_3$), from the half metal ferromagnetic electrode, $La_{0.63}Sr_{0.37}MnO_3$ (LSMO), under an external magnetic field, enabling their use in spin-light emitting diodes (spin-LEDs) (Fig. 13b).[60] The ferromagnetic half-metallic nature of LSMO has a spin polarization ability close to 100% at the Fermi level. It has been suggested that Sr segregation and the surface layer made up of SrO and $SrCO_3$ play an important role in spin injection properties at the hybrid interfacial region, probably forming a tunneling barrier at the interface.[61] However, it is also well-known that the spin injection efficiency (γ) at the semiconductor/ferromagnetic interface is proportional to the ratio of their conductivities (σ) (σ_{SC}/σ_{FM}). The conductivity of the ferromagnetic electrode (FM) is several orders of magnitude higher than that of the semiconductor (SC), which in turn makes $\gamma << 1$, resulting in loss of spin information at the SC/FM interface. Without the use of an external magnetic field or ferromagnetic contact, a spin light emitting diode (spin-LED) can operate at room temperature using a chiral organic molecule which can be explained by the CISS effect, and this is indeed a great achievement in optoelectronic applications.

The effective spin injection from chiral halide perovskite (R/S-$MBA)_2BX_4$ (MBA = α-methylbenzylammonium; B = Sn, Pb; X = I, Br) layers into commercially workable III-Vs based semiconductors (*e.g.*, Si, Ge, *etc.*) has been demonstrated. It has been observed that the injected current was spin-polarized, and the detection of circularly polarized light emission confirmed the spin accumulation in the III-V-based semiconductor. Furthermore, the conductivity mismatch, observed between the ferromagnetic electrode and organic semiconductor has been successfully overcome. In addition, the spin orientation formed by the CISS mechanism is parallel to the direction of the current and the emitted light is also aligned with the current direction because of the small escape cone of the III-V-based semiconductor. Thus, it enhances spin-to-light conversion and satisfies the optical selection rules that require the circularly polarised light helicity to be parallel to the emission direction. Kim and others have demonstrated control over charge, spin, and light by incorporating the chiral metal-halide perovskite ((R-/S-$MBA)_2PdI_4$) hybrid semiconductor, which shows the CISS effect (Fig. 14).[62] It has been observed that the circularly polarised electroluminescence (CP-EL), which is emitted through the spin-LED has a spin-polarized current of >80% with 2.6% efficiency at room temperature, achieved by controlling the intensity of CP-El and proper alignment. They studied spin-polarized charge transport in the CISS layer and CISS/nonchiral nanocrystal (NC) heterostructure by mCP-AFM and observed a higher current for ITO/m-PEDOT: PSS/$(R\text{-MBA})_2PbI_4/CsPbI_3$ NC films when the tip was magnetized upwards compared to when the tip was magnetized either downwards or left nonmagnetized. The reverse observation was noted for ITO/m-PEDOT: PSS/$(S\text{-MBA})_2PbI_4/CsPbI_3$ NC films (Fig. 15).

Oxygen evolution reaction and oxygen reduction reaction in chiral materials

Organic–inorganic hybrid materials have been extensively used in both the oxygen evolution reaction and oxygen reduction reaction. Specifically, efficient electrocatalysts, for electrochemical water-splitting, are very crucial for future sustainable energy and carbon neutrality processes. There is a relationship

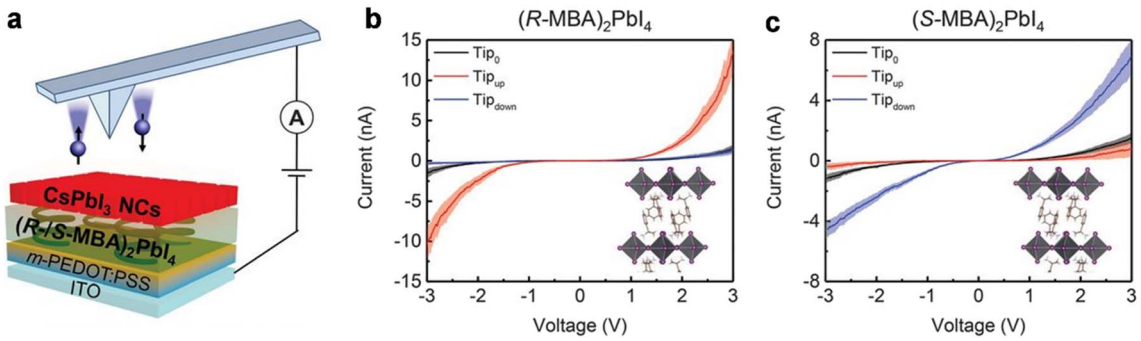

Fig. 15 (a) Schematic representation of mCP-AFM measurements of the device in the form of ITO/m-PEDOT: PSS/(R-/S-$MBA)_2PbI_4/CsPbI_3$ NC films. Current *vs.* voltage plots of the device using (b) (R-$MBA)_2PbI_4$ and (c) (S-$MBA)_2PbI_4$ at room temperature. Insets display the crystal structure of (R-/S-$MBA)_2PbI_4$. Tip_0 represents the nonmagnetized AFM tip; Tip_{up} represents the AFM tip magnetized up; Tip_{down} represents the AFM tip magnetized down. Figures are adapted with permission from ref. 62.

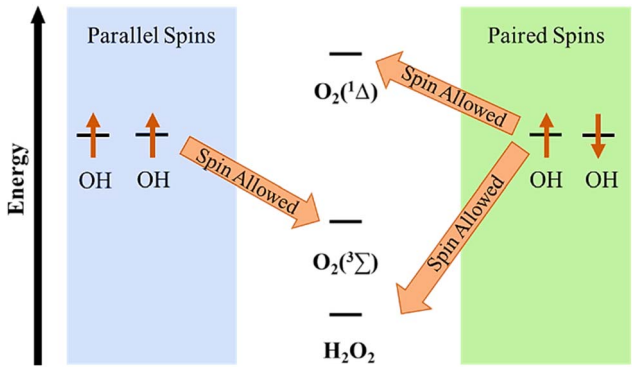

Fig. 16 Proposed energy diagram as described in the literature.[69] The figure is reconstructed from ref. 69.

between the activity of an electrocatalyst and its binding energy with reaction intermediates. The conventional way to increase the activity is to optimize the binding energy of the catalyst which should be optimal according to the Sabatier principle. However, the sluggish kinetics and high overpotential of the OER limit the extensive use of electrocatalytic water-splitting in different aspects of renewable energy applications. Hence, beyond the thermodynamic limitations that ignore the role of spin, some unconventional approaches have been investigated for the improvement of the OER. As the ground state of diatomic oxygen is a triplet, spin constraints should influence the elementary reaction steps. By spin-polarized electron transfer, the formation of reaction intermediates can be controlled and the efficiency of the OER can also be improved. Hence, chiral organic–inorganic hybrid materials have been explored as one of the solutions for the reduction of high overpotential, controlling the formation of side products and increasing the faradaic efficiency.[38,63–68] Using nonmagnetic or achiral electrodes, the reaction proceeds through a singlet potential surface, resulting in the formation of excited state oxygen and thus creating an energy barrier between the two energy states. Besides, chiral or magnetic electrodes, where electrons' spins are coaligned might help overcome this issue (Fig. 16). Thus, the activity of OER and ORR catalysts can be improved beyond the volcano limit by chiral molecular functionalization. Besides, it offers greater versatility with sustainable electron spin polarization and can be implemented into a variety of catalysts, irrespective of their electronic (magnetic) properties under different reaction conditions without affecting the catalyst's composition and surface reconstruction.[26,30,69] In this respect, chiral Fe_3O_4 nanoparticles (NPs) have been found to show superior catalytic activity towards the oxygen evolution reaction by exhibiting lower overpotential and minimizing H_2O_2 production. Significant current density has been obtained in the range of 10 mA cm^{-2} which is much higher than the previously reported values for TiO_2 coated with a chiral molecules/film monolayer, where the current density was observed to be below 1 mA cm^{-2}.[70] For chiral modification, Fe_2O_3 nanoparticles were encapsulated with chiral amino acids and peptide molecules.[70] The results shown in Fig. 17 reveal that the current density obtained from the chiral catalyst is much higher than that of the achiral one. Another study demonstrated that chiral copper oxide films were employed to improve the chemical selectivity for electrocatalytic water-splitting.[69] The chiral

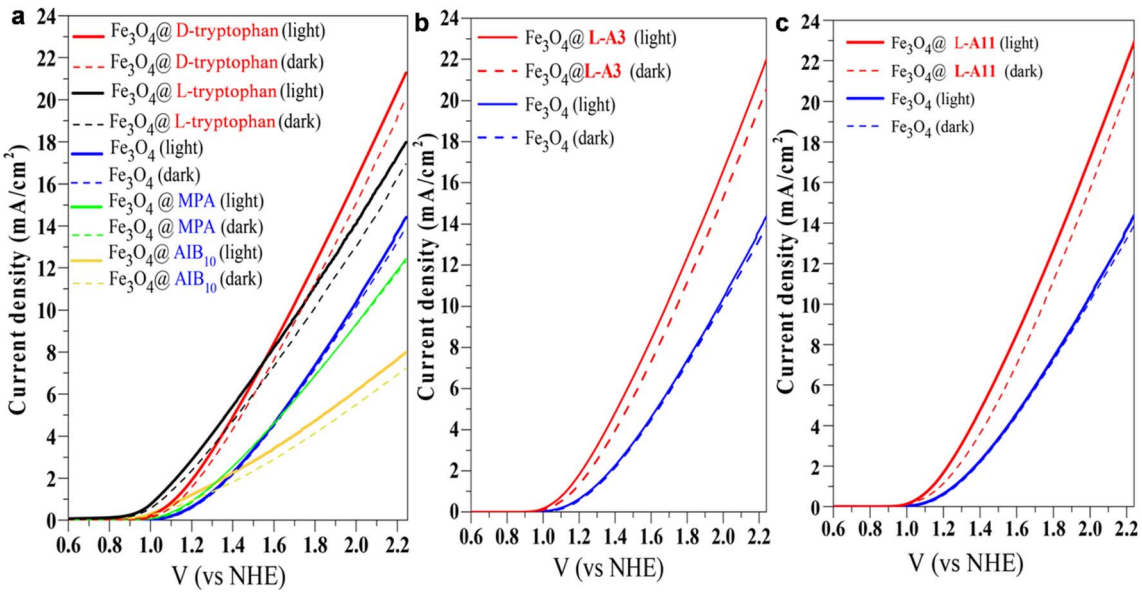

Fig. 17 (a–c) Linear sweep voltammetry plots of Fe_2O_3 nanoparticles encapsulated with different chiral and achiral molecules. Electrochemical water splitting was carried out using 0.1 M KOH solution (pH 13) as the electrolyte and a saturated calomel electrode as the reference electrode, with a scanning rate of 20 mV s^{-1}. For chiral modification, L-and D-tryptophan, L-A3 (SH–$(CH_2)_2$–NH–(Ala-AIB)$_3$-COOH, chiral), and L-A11(SH-$(CH_2)_2$–NH–(Ala-AIB)$_{11}$–NH_2, chiral) were used whereas for achiral modification, 3-mercaptopropionic acid and AIB10 (NH–$(CH_2)_2$–SH–$(AIB)_{10}$–NH_2, achiral) were used. 'Ala' denotes alanine and 'AIB' denotes α-aminoisobutyric acid. The figure is adapted with permission from ref. 70 (copyright 2018, American Chemical Society).

CuO films act as electron spin filters, developed on the electrode surface by an electrodeposition method using a chiral Cu(II) complex containing electrolyte solution. The work revealed that spin-polarised electrons favored triplet oxygen production, suppressing the H_2O_2 byproduct production and resulting in low overpotential, and high current density. A similar observation has been found for an electrochemically deposited chiral cobalt oxide-coated anode.[71] Vadakkayil *et al.* also demonstrated in detail that doping iron into the chiral organic molecule modified cobalt oxide decreases the overpotential for the OER.[72]

Recently, another interesting work by Nair *et al.* demonstrated the synergistic effects of the inherent magnetic properties of iron oxide nanoparticles and chiral molecular functionalization on OER activity.[73] In this study, ferrimagnetic (f) and superparamagnetic (s) Fe_3O_4 catalysts were synthesized, and an enhancement in OER activity was observed for both magnetic particles upon applying an external magnetic field due to spin-selectivity. In addition, s-Fe_3O_4 was functionalized with chiral organic molecules *R*- and *S*-1,2-diaminopropane dihydrochloride (DPDC), resulting in 42% spin-polarization, which significantly enhances the OER activity by increasing the current density and lowering the onset potential as depicted in Fig. 18.

A recent study showed that chiral modification of iridium nanoparticles also boosts the current density for the OER with respect to pristine metal nanoparticles and achiral particles.[74] Feng *et al.* explored that a chiral amorphous Fe–Ni electrocatalyst synthesized by an electrodeposition method enhances the electrochemical oxygen evolution with respect to its achiral analog by a spin-polarized charge transfer process.[75] In addition to this single metal oxide-based catalyst, two-dimensional transition metal-based oxo hydroxides are also explored as chiral catalysts by integrating them with chiral organic molecules. Recently, Lingenfelder *et al.* reported that integrating chiral fused thiadiazol-helicene molecules with 2D Ni- and Ni, Fe-based catalysts, spin polarization can be introduced into the anode that helps in augmentation of the OER activity in alkaline media.[76] It was demonstrated that Fe doping in the catalysts along with Fe impurities in the electrolytes efficiently enhanced the OER activity (Fig. 19). The study suggests that the bonding strength and charge transfer between adsorbed oxygen and the chiral catalyst are strongly influenced by the electron's spin. In this study, the gold surface was functionalized with a chiral helicene molecule and then a NiFe-containing catalyst was coated on top of the chiral molecule (Fig. 19c). The superior catalytic activity results from the spin-polarization of the catalyst surface.

Apart from the OER, chiral hybrid materials are also found to be very effective for the oxygen reduction reaction process. With the growing interest in clean energy technologies like fuel cells, and metal–air batteries, the electrocatalyst for the oxygen

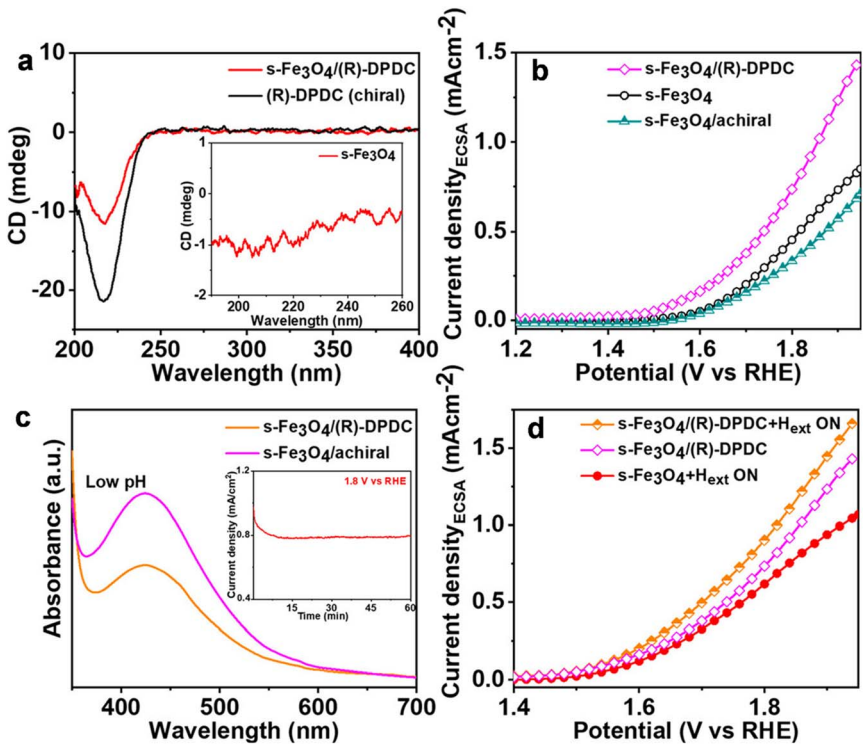

Fig. 18 (a) Circular dichroism (CD) spectra of chiral DPDC molecules and chiral functionalized superparamagnetic (s) Fe_3O_4 catalysts. (b) Linear sweep voltammetry plots exhibiting the augmented electrochemical activity of the chiral catalyst. (c) UV-vis absorption spectra for the estimation of H_2O_2 detection using chiral and achiral catalysts. (d) LSV curves of the chiral s-Fe_3O_4 catalyst under an external magnetic field. DPDC was used for chiral modification and ethylene diamine was used for achiral modification. Figures are adapted with permission from ref. 73 (copyright 2023, American Chemical Society).

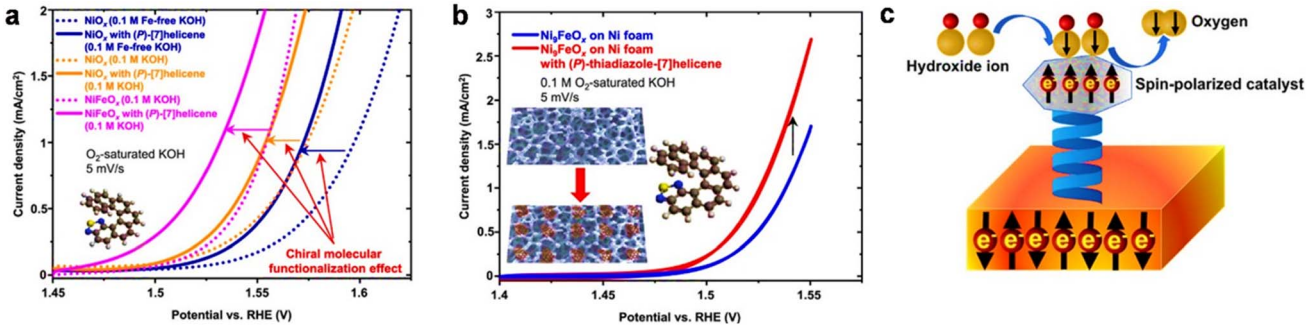

Fig. 19 Current density *vs.* applied potential plots (a) to check the effect of chiral modification on NiO_x islands in Fe-free KOH, NiO_x islands in unpurified KOH, and $NiFeO_x$ islands in unpurified KOH and (b) to check the chiral molecular functionalization enhancement at Ni_xFeO_x deposited on Ni foam. (c) Proposed mechanism of the OER. Figures are adapted with permission from ref. 76 (copyright @2022, Nature Communications).

reduction reaction (ORR) is also imperative for ensuring the sustainability of this type of future clean energy. As with the OER, spin selection limitation is also associated with the ORR as the diatomic oxygen is involved as the substrate here.[77] Sang and others compared two electrodes coated with self-assembled monolayer (SAM) of achiral 3-mercaptopropionic acid (MPA) and chiral L-cysteine and found an approximately 0.17 V shift in the onset potential for reduction despite the two molecules having the same length and a resembling structure (Fig. 20a). They further studied the chirality effect on gold (Au) and platinum (Pt) nanoparticles (NPs). By comparing chiral gold NPs and achiral ones, they found that chiral Au NPs exhibited approximately 178 mV lower onset potential than their achiral counterparts (Fig. 20b) and chiral Pt NPs exhibited 80 mV lower onset potential compared to achiral Pt NPs and 30 mV lower onset potential compared to commercial Pt/C for the ORR

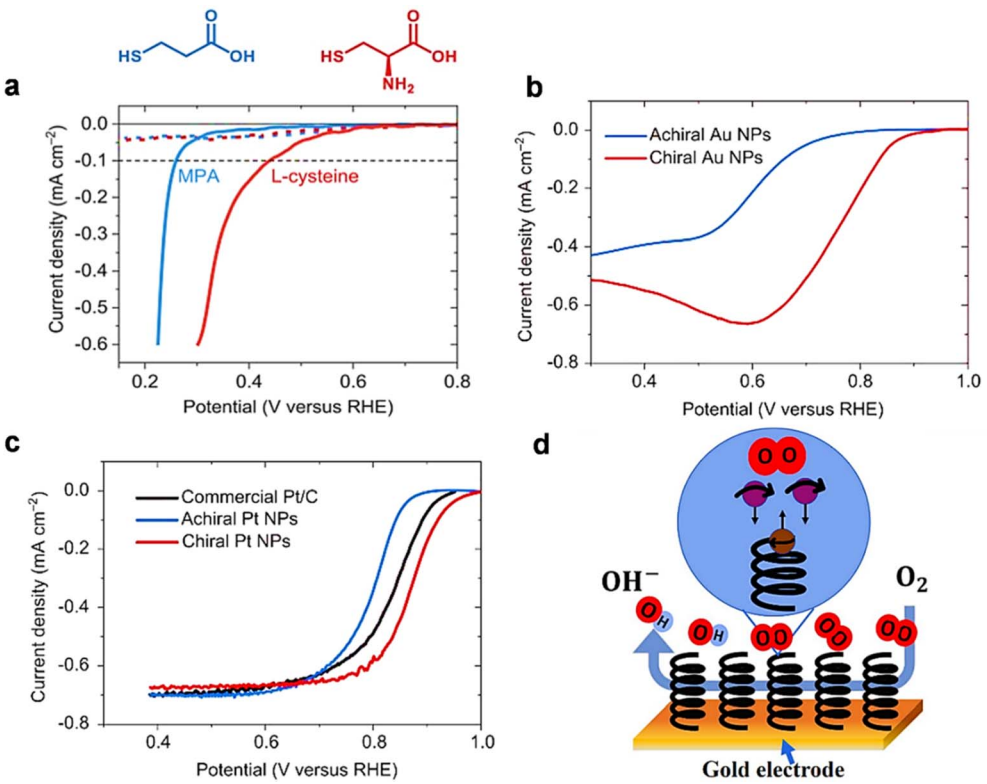

Fig. 20 (a). LSV plots for the electrode coated with achiral molecules (blue curves) and chiral molecules using (red curves) in N_2 (dashed lines) and O_2 (solid lines)-saturated 0.1 M KOH (pH 13) aqueous solution as electrolyte. Current density *vs.* applied potential plots obtained from (b). Chiral and achiral Au NPs coated electrodes in oxygen-saturated 0.1 M KOH aqueous solution at a scanning speed of 50 mV s^{-1} under static conditions (c). Chiral and achiral Pt NPs and commercial catalyst Pt/C coated electrodes in air-saturated 0.1 M KOH solution at a rotation speed of 1500 rpm and a sweep rate of 5 mV s^{-1} using a rotating disc electrode. Figures (a–c) are adapted with permission from ref. 77 (d). Schematic representation of a chiral molecule-modified electrode that favors the ORR through a spin-specific way. The scheme is reconstructed from ref. 77 (copyright 2022, PNAS).

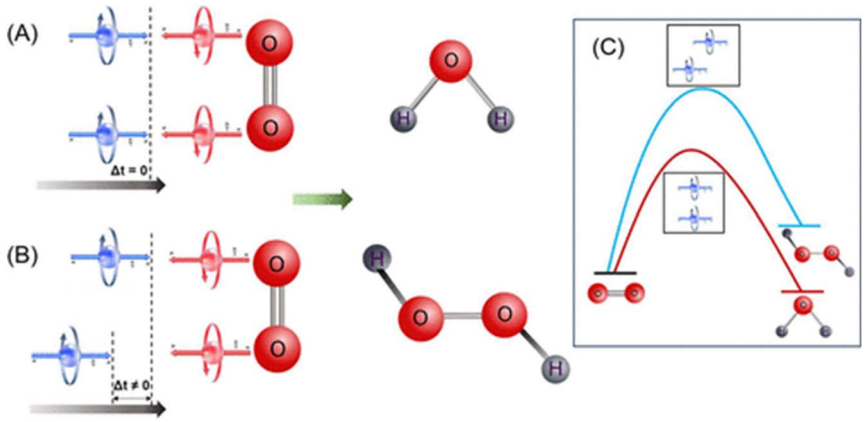

Fig. 21 (A). Two electrons form a coherent pair, and it drives the ORR to produce water. (B) Two electrons do not form a coherent pair, and it drives the ORR to produce hydrogen peroxide. (C) When two electrons are not coherent the oxygen reduction will follow a high-energy pathway. The figure is adapted from ref. 78 (copyright 2024, American Chemical Society).

process (Fig. 20c). The proposed mechanism is displayed in Fig. 20d. Recently Gupta *et al.* reported that coherence affects the rate of the oxygen reduction reaction demonstrating that different thicknesses of chiral molecular coatings possess different catalytic activities.[78] They proposed a model indicating that during the ORR process, when two electrons form a coherent pair and are inserted coherently into oxygen molecules, the rate of the reaction becomes faster, and the production of water is preferred. However, when two electrons are not coherent, *i.e.*, the electrons are not transferred coherently into oxygen molecules and subsequently hydrogen peroxide will be produced. The theoretical model proposed here is shown in Fig. 21.

The laccase-modified cathode has been shown to combine two strategies to promote effective electron transfer: (1) "direct electron transfer" and (2) "mediated electron transfer" by the Kashiwagi group in their enzymatic biofuel cell.[79] Previously it has already been stated that some of the electrochemical redox reactions depend on electron spin orientation.[80] The study demonstrates that the chirality of the oligopeptide linker that links the enzyme to the surface influences the ORR efficiency of the laccase-modified electrode. However, the Cu(II) complex with an amino-acid derivative with/without an azobenzene moiety as a mediator enhanced the electrochemical current by improving the electron transport between the enzyme and the cathode. Hence, it should be appreciated that a chiral organic molecule may not compete with the commercially available inorganic catalyst for both the OER and ORR but its integration with top-performing catalysts will enhance their efficiency.

Future outlook

Over the last decade, the CISS effect has experienced substantial growth, with researchers exploring numerous directions and making significant strides. Through experiments and theoretical studies, scientists worldwide have observed the presence of different spin polarization in chiral molecules when one contact is magnetic, and the magnetization is switched. The CISS effect manifests in a wide range of temperatures and can be seen in single molecules, monolayers, and thin films. This research shows great promise in providing new insights into various fields, including chemistry, biology, and physics. As fundamental studies continue, they are creating new avenues for CISS research in diverse fields like emergent magnetism, spin-controlled chemistry, and the origin of homochirality in biology. Another crucial area of exploration is the role of CISS in quantum information science (QIS). Developing materials that exhibit quantum properties at room temperature is a significant goal of QIS, and CISS presents a new approach. While the CISS effect has offered several technological advancements from magnetoresistance devices to photovoltaics, light emitting diodes, and catalytic processes, certain limitations such as comprehensive theoretical models, material and experimental constraints, and sensitivity to environmental factors create hurdles for its commercial and industrial use. Several fundamental studies have been executed to overcome these limitations, providing an enhanced understanding of the CISS effect. Another important aspect is that continuous current measurements in the single-molecule junction have revealed chirality differences, consistent with the anticipated behavior of the CISS effect. These findings further affirm the occurrence of CISS at the single-molecule level. Nevertheless, these noteworthy results are not yet fully comprehended, and additional investigation is necessary to validate the conclusions. Therefore, to clarify and improve the fundamental principles underlying the CISS effect, more sophisticated measurement techniques are imperative. We maintain an optimistic outlook that the current and future research will unveil the CISS mechanism in the foreseeable future, thereby propelling CISS applications beyond current contemplation. Still, the full potential of CISS has yet to be determined and its implications cannot be fully projected at this stage. Therefore, it is vital to continue exploring the CISS effect to comprehend its full potential, and establish a clear mechanism that can pave the way for future discoveries.

Data availability

No primary research results, software, or code have been included and no new data were generated or analyzed as part of this review article.

Author contributions

Conceptualization & supervision: P. C. M.; writing— original draft: R. G., A. B., and R. Garg; writing—review and editing: P. C. M., A. K. M., and K. B. G.; funding acquisition: P. C. M., A. K. M., and K. B. G. All authors have read and agreed to the published version of the manuscript.

Conflicts of interest

The authors declare no competing interests related to this work.

Acknowledgements

R. Gupta thanks IIT Kanpur for a senior research fellowship. A. B. acknowledges the MHRD for a junior research fellowship. R. Garg thanks INST Mohali for a junior research fellowship. A. K. M. acknowledges financial support from the DST INSPIRE grant (DST/INSPIRE/04/2021/000055) and DAE-BRNS (Sanction No. 58/14/03/2024-BRNS). K. B. G. acknowledges the Start-up Research Grant (SRG/2022/000737) from SERB-India. P. C. M. acknowledges the Science and Engineering Research Board, New Delhi (Grant No. CRG/2022/005325).

References

1 E. Coronado, *Nat. Rev. Mater.*, 2020, **5**, 87–104.
2 R. Gupta, J. Pradhan, A. Haldar, C. Murapaka and P. C. Mondal, *Angew. Chem., Int. Ed.*, 2023, **62**, e202307458.
3 K. V. Raman, A. M. Kamerbeek, A. Mukherjee, N. Atodiresei, T. K. Sen, P. Lazić, V. Caciuc, R. Michel, D. Stalke, S. K. Mandal, S. Blügel, M. Münzenberg and J. S. Moodera, *Nature*, 2013, **493**, 509–513.
4 S. J. Wang, D. Venkateshvaran, M. R. Mahani, U. Chopra, E. R. McNellis, R. Di Pietro, S. Schott, A. Wittmann, G. Schweicher, M. Cubukcu, K. Kang, R. Carey, T. J. Wagner, J. N. M. Siebrecht, D. P. G. H. Wong, I. E. Jacobs, R. O. Aboljadayel, A. Ionescu, S. A. Egorov, S. Mueller, O. Zadvorna, P. Skalski, C. Jellett, M. Little, A. Marks, I. McCulloch, J. Wunderlich, J. Sinova and H. Sirringhaus, *Nat. Electron.*, 2019, **2**, 98–107.
5 M. Cinchetti, V. A. Dediu and L. E. Hueso, *Nat. Mater.*, 2017, **16**, 507–515.
6 L. Guo, X. Gu, X. Zhu and X. Sun, *Adv. Mater.*, 2019, **31**, 1805355.
7 K. Michaeli, N. Kantor-Uriel, R. Naaman and D. H. Waldeck, *Chem. Soc. Rev.*, 2016, **45**, 6478–6487.
8 V. Varade, T. Z. Markus, K. Vankayala, N. Friedman, M. Sheves, D. H. Waldeck and R. Naaman, *Phys. Chem. Chem. Phys.*, 2017, **20**, 1091–1097.
9 R. Naaman, Y. Paltiel and D. H. Waldeck, *J. Phys. Chem. Lett.*, 2020, **11**, 3660–3666.
10 R. Naaman and D. H. Waldeck, *Annu. Rev. Phys. Chem.*, 2015, **66**, 263–281.
11 B. P. Bloom, Y. Paltiel, R. Naaman and D. H. Waldeck, *Chem. Rev.*, 2024, **124**, 1950–1991.
12 P. C. Mondal, C. Fontanesi, D. H. Waldeck and R. Naaman, *Acc. Chem. Res.*, 2016, **49**, 2560–2568.
13 S. H. Yang, R. Naaman, Y. Paltiel and S. S. P. Parkin, *Nat. Rev. Phys.*, 2021, **3**, 328–343.
14 K. Ray, S. P. Ananthavel, D. H. Waldeck and R. Naaman, *Science*, 1999, **283**, 814–816.
15 B. P. Bloom, Z. Chen, H. Lu and D. H. Waldeck, *Natl. Sci. Rev.*, 2024, **11**, nwae212.
16 F. Evers, A. Aharony, N. Bar-Gill, O. Entin-Wohlman, P. Hedegård, O. Hod, P. Jelinek, G. Kamieniarz, M. Lemeshko, K. Michaeli, V. Mujica, R. Naaman, Y. Paltiel, S. Refaely-Abramson, O. Tal, J. Thijssen, M. Thoss, J. M. van Ruitenbeek, L. Venkataraman, D. H. Waldeck, B. Yan and L. Kronik, *Adv. Mater.*, 2022, **34**, 2106629.
17 D. Qi, A. Kenaan, D. Cui and J. Song, *Nano Energy*, 2018, **52**, 142–152.
18 J. Fransson, *Isr. J. Chem.*, 2022, **62**, e202200046.
19 R. Naaman, Y. Paltiel and D. H. Waldeck, *Nat. Rev. Chem*, 2019, **3**, 250–260.
20 C. D. Aiello, J. M. Abendroth, M. Abbas, A. Afanasev, S. Agarwal, A. S. Banerjee, D. N. Beratan, J. N. Belling, B. Berche, A. Botana, J. R. Caram, G. L. Celardo, G. Cuniberti, A. Garcia-Etxarri, A. Dianat, I. Diez-Perez, Y. Guo, R. Gutierrez, C. Herrmann, J. Hihath, S. Kale, P. Kurian, Y.-C. Lai, T. Liu, A. Lopez, E. Medina, V. Mujica, R. Naaman, M. Noormandipour, J. L. Palma, Y. Paltiel, W. Petuskey, J. C. Ribeiro-Silva, J. J. Saenz, E. J. G. Santos, M. Solyanik-Gorgone, V. J. Sorger, D. M. Stemer, J. M. Ugalde, A. Valdes-Curiel, S. Varela, D. H. Waldeck, M. R. Wasielewski, P. S. Weiss, H. Zacharias and Q. H. Wang, *ACS Nano*, 2022, **16**, 4989–5035.
21 R. Naaman and D. H. Waldeck, *J. Phys. Chem. Lett.*, 2012, **3**, 2178–2187.
22 K. Banerjee-Ghosh, S. Ghosh, H. Mazal, I. Riven, G. Haran and R. Naaman, *J. Am. Chem. Soc.*, 2020, **142**, 20456–20462.
23 S. Ghosh, K. Banerjee-Ghosh, D. Levy, D. Scheerer, I. Riven, J. Shin, H. B. Gray, R. Naaman and G. Haran, *Proc. Natl. Acad. Sci. U. S. A.*, 2022, **119**, e2204735119.
24 S. Ghosh, K. Banerjee-Ghosh, D. Levy, I. Riven, R. Naaman and G. Haran, *J. Phys. Chem. Lett.*, 2021, **12**, 2805–2808.
25 S. S. Skourtis, D. N. Beratan, R. Naaman, A. Nitzan and D. H. Waldeck, *Phys. Rev. Lett.*, 2008, **101**, 238103.
26 M. Kettner, V. V. Maslyuk, D. Nürenberg, J. Seibel, R. Gutierrez, G. Cuniberti, K. H. Ernst and H. Zacharias, *J. Phys. Chem. Lett.*, 2018, **9**, 2025–2030.
27 K. Michaeli, D. N. Beratan, D. H. Waldeck and R. Naaman, *Proc. Natl. Acad. Sci. U. S. A.*, 2019, **116**, 5931–5936.
28 J. Fransson, *Phys. Rev. B*, 2020, **102**, 235416.
29 T. K. Das, R. Naaman and J. Fransson, *Adv. Mater.*, 2024, **36**, 2313708.

30 V. Kiran, S. P. Mathew, S. R. Cohen, I. Hernández Delgado, J. Lacour and R. Naaman, *Adv. Mater.*, 2016, **28**, 1957–1962.
31 M. R. Safari, F. Matthes, C. M. Schneider, K.-H. Ernst and D. E. Bürgler, *Small*, 2024, **20**, 2308233.
32 M. Suda, Y. Thathong, V. Promarak, H. Kojima, M. Nakamura, T. Shiraogawa, M. Ehara and H. M. Yamamoto, *Nat. Commun.*, 2019, **10**, 2455.
33 Q. Zhu, W. Danowski, A. K. Mondal, F. Tassinari, C. L. F. van Beek, G. H. Heideman, K. Santra, S. R. Cohen, B. L. Feringa and R. Naaman, *Adv. Sci.*, 2021, **8**, 2101773.
34 S. Mishra, S. Pirbadian, A. K. Mondal, M. Y. El-Naggar and R. Naaman, *J. Am. Chem. Soc.*, 2019, **141**, 19198–19202.
35 D. Mishra, T. Z. Markus, R. Naaman, M. Kettner, B. Göhler, H. Zacharias, N. Friedman, M. Sheves and C. Fontanesi, *Proc. Natl. Acad. Sci. U. S. A.*, 2013, **110**, 14872–14876.
36 R. Gupta, H. V. Chinnasamy, D. Sahu, S. Matheshwaran, C. Sow and P. C. Mondal, *J. Chem. Phys.*, 2023, **159**, 024708.
37 P. C. Mondal, N. Kantor-Uriel, S. P. Mathew, F. Tassinari, C. Fontanesi and R. Naaman, *Adv. Mater.*, 2015, **27**, 1924–1927.
38 W. Mtangi, F. Tassinari, K. Vankayala, A. Vargas Jentzsch, B. Adelizzi, A. R. A. Palmans, C. Fontanesi, E. W. Meijer and R. Naaman, *J. Am. Chem. Soc.*, 2017, **139**, 2794–2798.
39 C. Kulkarni, A. K. Mondal, T. K. Das, G. Grinbom, F. Tassinari, M. F. J. Mabesoone, E. W. Meijer and R. Naaman, *Adv. Mater.*, 2020, **32**, 1–7.
40 S. Mishra, A. K. Mondal, E. Z. B. Smolinsky, R. Naaman, K. Maeda, T. Nishimura, T. Taniguchi, T. Yoshida, K. Takayama and E. Yashima, *Angew. Chem., Int. Ed.*, 2020, **132**, 14779–14784.
41 A. K. Mondal, M. D. Preuss, M. L. Ślęczkowski, T. K. Das, G. Vantomme, E. W. Meijer and R. Naaman, *J. Am. Chem. Soc.*, 2021, **143**, 7189–7195.
42 A. T. Rösch, Q. Zhu, J. Robben, F. Tassinari, S. C. J. Meskers, R. Naaman, A. R. A. Palmans and E. W. Meijer, *Chem.–A Eur. J.*, 2021, **27**, 298–306.
43 J. Labella, D. K. Bhowmick, A. Kumar, R. Naaman and T. Torres, *Chem. Sci.*, 2023, **14**, 4273–4277.
44 N. Giaconi, L. Poggini, M. Lupi, M. Briganti, A. Kumar, T. K. Das, A. L. Sorrentino, C. Viglianisi, S. Menichetti, R. Naaman, R. Sessoli and M. Mannini, *ACS Nano*, 2023, **17**, 15189–15198.
45 D. Y. Zhang, Y. Sang, T. K. Das, Z. Guan, N. Zhong, C. G. Duan, W. Wang, J. Fransson, R. Naaman and H. B. Yang, *J. Am. Chem. Soc.*, 2023, **145**, 26791–26798.
46 G. Gotesman, D. H. Waldeck and R. Naaman, *J. Phys. Chem. A*, 2009, **113**, 7213–7217.
47 S. Majumdar, G. Śliwiński and Y. Garcia, in *Hybrid Organic-Inorganic Interfaces*, 2018, pp. 301–353.
48 C. Taliani, V. Dediu, F. Biscarini, M. Cavallini, M. Murgia, G. Ruani and P. Nozar, *Phase Transitions*, 2002, **75**, 1049–1058.
49 F. Li, T. Li, F. Chen and F. Zhang, *Sci. Rep.*, 2015, **5**, 9355.
50 B. P. Bloom, V. Kiran, V. Varade, R. Naaman and D. H. Waldeck, *Nano Lett.*, 2016, **16**, 4583–4589.
51 A. K. Mondal, N. Brown, S. Mishra, P. Makam, D. Wing, S. Gilead, Y. Wiesenfeld, G. Leitus, L. J. W. Shimon, R. Carmieli, D. Ehre, G. Kamieniarz, J. Fransson, O. Hod, L. Kronik, E. Gazit and R. Naaman, *ACS Nano*, 2020, **14**, 16624–16633.
52 T. Kumar Das, A. K. Mondal, O. S. Tiwari, P. Makam, G. Leitus, E. Gazit, F. Claudio and R. Naaman, *Phys. Chem. Chem. Phys.*, 2023, **25**, 22124–22129.
53 J. M. Abendroth, D. M. Stemer, B. P. Bloom, P. Roy, R. Naaman, D. H. Waldeck, P. S. Weiss and P. C. Mondal, *ACS Nano*, 2019, **13**, 4928–4946.
54 Y. Zhang, T. P. Basel, B. R. Gautam, X. Yang, D. J. Mascaro, F. Liu and Z. V. Vardeny, *Nat. Commun.*, 2012, **3**, 1043.
55 D. Giovanni, H. Ma, J. Chua, M. Grätzel, R. Ramesh, S. Mhaisalkar, N. Mathews and T. C. Sum, *Nano Lett.*, 2015, **15**, 1553–1558.
56 B. A. Rosales, K. Schutt, J. J. Berry and L. M. Wheeler, *ACS Energy Lett.*, 2023, **8**, 1705–1715.
57 K. J. Savill, A. M. Ulatowski and L. M. Herz, *ACS Energy Lett.*, 2021, **6**, 2413–2426.
58 R. Das, D. Swain, A. Mahata, D. Prajapat, S. K. Upadhyay, S. Saikia, V. R. Reddy, F. De Angelis and D. D. Sarma, *Chem. Mater.*, 2024, **36**, 1891–1898.
59 D. Sun, T. P. Basel, B. R. Gautam, W. Han, X. Jiang, S. S. P. Parkin and Z. Valy Vardeny, *Appl. Phys. Lett.*, 2013, **103**, 42411.
60 J. Wang, C. Zhang, H. Liu, R. McLaughlin, Y. Zhai, S. R. Vardeny, X. Liu, S. McGill, D. Semenov, H. Guo, R. Tsuchikawa, V. V. Deshpande, D. Sun and Z. V. Vardeny, *Nat. Commun.*, 2019, **10**, 1–6.
61 M. P. De Jong, V. A. Dediu, C. Taliani and W. R. Salaneck, *J. Appl. Phys.*, 2003, **94**, 7292–7296.
62 Y.-H. Kim, Y. Zhai, H. Lu, X. Pan, C. Xiao, E. A. Gaulding, S. P. Harvey, J. J. Berry, Z. V. Vardeny, J. M. Luther and M. C. Beard, *Science*, 2021, **371**, 1129–1133.
63 W. Mtangi, V. Kiran, C. Fontanesi and R. Naaman, *J. Phys. Chem. Lett.*, 2015, **6**, 4916–4922.
64 F. Tassinari, K. Banerjee-Ghosh, F. Parenti, V. Kiran, A. Mucci and R. Naaman, *J. Phys. Chem. C*, 2017, **121**, 15777–15783.
65 J. Liu, Y. Liu, N. Liu, Y. Han, X. Zhang, H. Huang, Y. Lifshitz, S.-T. Lee, J. Zhong and Z. Kang, *Science*, 2015, **347**, 970–974.
66 J. A. Seabold and K. S. Choi, *Chem. Mater.*, 2011, **23**, 1105–1112.
67 H. Gajapathy, S. Bandaranayake, E. Hruska, A. Vadakkayil, B. P. Bloom, S. Londo, J. McClellan, J. Guo, D. Russell, F. M. F. de Groot, F. Yang, D. H. Waldeck, M. Schultze and L. R. Baker, *Chem. Sci.*, 2024, **15**, 3300–3310.
68 U. Utkarsh, S. R. Pramatha, A. Balo, U. K. Gosh, K. V. Rao and K. B. Ghosh, *J. Mater. Chem. A*, 2024, **12**, 20354–20363.
69 K. B. Ghosh, W. Zhang, F. Tassinari, Y. Mastai, O. Lidor-Shalev, R. Naaman, P. Möllers, D. Nürenberg, H. Zacharias, J. Wei, E. Wierzbinski and D. H. Waldeck, *J. Phys. Chem. C*, 2019, **123**, 3024–3031.
70 W. Zhang, K. Banerjee-Ghosh, F. Tassinari and R. Naaman, *ACS Energy Lett.*, 2018, **3**, 2308–2313.
71 S. Ghosh, B. P. Bloom, Y. Lu, D. Lamont and D. H. Waldeck, *J. Phys. Chem. C*, 2020, **124**, 22610–22618.

72 A. Vadakkayil, C. Clever, K. N. Kunzler, S. Tan, B. P. Bloom and D. H. Waldeck, *Nat. Commun.*, 2023, **14**, 1067.
73 A. N. Nair, S. Fernandez, M. Marcos-Hernández, D. R. Romo, S. R. Singamaneni, D. Villagran and S. T. Sreenivasan, *Nano Lett.*, 2023, **23**, 9042–9049.
74 C. J. Mingoes, B. C. Schroeder and A. B. Jorge Sobrido, *ACS Mater. Au*, 2024, **4**, 204–213.
75 T. Feng, W. Chen, J. Xue, F. Cao, Z. Chen, J. Ye, C. Xiao and H. Lu, *Adv. Funct. Mater.*, 2023, **33**, 2215051.
76 Y. Liang, K. Banjac, K. Martin, N. Zigon, S. Lee, N. Vanthuyne, F. A. Garcés-Pineda, J. R. Galán-Mascarós, X. Hu, N. Avarvari and M. Lingenfelder, *Nat. Commun.*, 2022, **13**, 1–9.
77 Y. Sang, F. Tassinari, K. Santra, W. Zhang, C. Fontanesi, B. P. Bloom, D. H. Waldeck, J. Fransson and R. Naaman, *Proc. Natl. Acad. Sci. U. S. A.*, 2022, **119**, e2202650119.
78 A. Gupta, A. Kumar, D. K. Bhowmick, C. Fontanesi, Y. Paltiel, J. Fransson and R. Naaman, *J. Phys. Chem. Lett.*, 2023, **14**, 9377–9384.
79 K. Kashiwagi, F. Tassinari, T. Haraguchi, K. Banerjee-Gosh, T. Akitsu and R. Naaman, *Symmetry*, 2020, **12**, 808.
80 P. C. Mondal, C. Fontanesi, D. H. Waldeck and R. Naaman, *ACS Nano*, 2015, **9**, 3377–3384.